

Occurrence Rates of Planets orbiting FGK Stars: Combining Kepler DR25, Gaia DR2 and Bayesian Inference

DANLEY C. HSU,^{1,2,3,4} ERIC B. FORD,^{1,2,3,4} DARIN RAGOZZINE,⁵ AND KEIR ASHBY⁵

¹Department of Astronomy & Astrophysics, 525 Davey Laboratory, The Pennsylvania State University, University Park, PA, 16802, USA

²Center for Exoplanets and Habitable Worlds, 525 Davey Laboratory, The Pennsylvania State University, University Park, PA, 16802, USA

³Center for Astrostatistics, 525 Davey Laboratory, The Pennsylvania State University, University Park, PA, 16802, USA

⁴Institute for CyberScience, The Pennsylvania State University

⁵Department of Physics & Astronomy, N283 ESC, Brigham Young University, Provo, UT 84602, USA

ABSTRACT

We characterize the occurrence rate of planets, ranging in size from $0.5\text{--}16 R_{\oplus}$, orbiting FGK stars with orbital periods from 0.5–500 days. Our analysis is based on results from the “DR25” catalog of planet candidates produced by NASA’s Kepler mission and stellar radii from Gaia “DR2”. We incorporate additional Kepler data products to accurately characterize the the efficiency of planets being recognized as a “threshold crossing events” (TCE) by Kepler’s Transiting Planet Search pipeline *and* labeled as a planet candidate by the robovetter. Using a hierarchical Bayesian model, we derive planet occurrence rates for a wide range of planet sizes and orbital periods. For planets with sizes $1\text{--}1.75 R_{\oplus}$ and orbital periods of 237–500 days, we find a rate of planets per FGK star of $0.24^{+0.11}_{-0.10}$ (68.3% credible interval). While the true rate of such planets could be lower by a factor of ~ 2 (primarily due to potential contamination of planet candidates by false alarms), the upper limits on the occurrence rate of such planets are robust to $\sim 10\%$. We recommend that mission concepts aiming to characterize potentially rocky planets in or near the habitable zone of sun-like stars prepare compelling science programs that would be robust for a true rate in the range $f_{R,P} = 0.05\text{--}0.51$ for $1\text{--}1.75 R_{\oplus}$ planets with orbital periods in 237–500 days, or a differential rate of $\Gamma_{\oplus} \equiv (d^2 f) / [d(\ln P) d(\ln R_p)] = 0.11\text{--}1.2$.

Keywords: methods: data analysis — methods: statistical — catalogs — planetary systems — stars: statistics

1. INTRODUCTION

In 2009, NASA’s Kepler mission began its mission to characterize the abundance and diversity of exoplanets. Four years of precise photometry of 189,516 target stars (as part of its exoplanet survey) allowed the Kepler project to identify 4,034 strong planet candidates via transit, over half of which have been confirmed by another method or validated based on detailed analyses of light curves and statistical considerations (Thompson et al. 2018). The Kepler mission was enormously successful, with an impressive array of discoveries, both anticipated and surprising. However, one of the primary goals of the mission, characterizing the frequency of Earth-size planets in or near the habitable zone of solar-like stars has remained elusive. A combination of factors, from intrinsic stellar variability to failure of Kepler’s reaction wheels, resulted in the Kepler data being sensitive to such planets around a small fraction of the stars surveyed and the detection efficiency of such planets depending sensitively on their host star properties. As a result, considerable care is necessary when inferring the rate of small planets near the habitable zone from Kepler data.

Several previous studies have estimated the rate of planets as a function of planet size and orbital period based on

Kepler data. Early studies had less data, but just as importantly, the accuracy of early studies were constrained by limited knowledge of the Kepler pipeline’s detection efficiency and the host star properties. Further complicating matters, Hsu et al. (2018) showed that one of the most common algorithms for estimating the planet occurrence rate was systematically biased for planets near Kepler’s detection threshold. While this bias is modest for much of the parameter space explored by Kepler, it can be of order unity for small planets near the habitable zone. Only a few recent studies analyzed the planet occurrence rates using a hierarchical Bayesian model, so as to avoid this bias (Foreman-Mackey et al. 2014; Burke et al. 2015; Hsu et al. 2018). Foreman-Mackey et al. (2014) inferred planet occurrence rates using a hierarchical Bayesian model with non-parametric model and a prior that favored the planet occurrence rate changing smoothly. This study analyzed a list of planet candidates from a non-standard pipeline that was restricted to finding a single planet around each star. Burke et al. (2015) inferred planet occurrence rates using a parametric model (i.e., power-law in planet size and orbital period) and a hierarchical Bayesian model. Hsu et al. (2018) inferred planet occurrence rates using a non-parametric model, a hierarchi-

cal Bayesian model and Approximate Bayesian Computing (ABC), and performed extensive tests on simulated catalogs to validate the algorithm. However, none of these studies made use of Kepler’s final planet catalog (known as DR25; Thompson et al. 2018), additional DR25 data products characterizing the detection pipeline’s efficiency (Christiansen 2017; Burke & Catanzarite 2017a,b,c; Coughlin 2017), or recent improvements in the knowledge of host star properties from the ESA’s Gaia mission (Gaia Collaboration et al. 2018). Recent studies indicate that the updates in stellar properties thanks to Gaia can have a significant effect on the inferred planet occurrence rate (Shabram et al. 2019, submitted).

In this manuscript, we report occurrence rates inferred using a hierarchical Bayesian model and Approximate Bayesian Computing (ABC), and incorporating several improvements relative to previous studies, including the DR25 catalog of planet candidates, updates to the host star properties from Gaia, and an improved model for the Kepler efficiency for detecting and vetting of planet candidates. We review the statistical methodology in §2.1 and describe improvements to our model since Hsu et al. (2018) in §2.2. In §3.1, we describe the selection of target stars, and present the resulting planet occurrence rates in §3.2. We conclude with a summary of key findings, implications for the rate of Earth-size planets in or near the habitable zone of FGK stars, and future of occurrence rate studies in §4.

2. METHODOLOGY

2.1. Approximate Bayesian Computation

Approximate Bayesian Computation (ABC) is a tool for performing Bayesian inference when the likelihood is not available. For example, ABC can be applied to perform inference using a hierarchical Bayesian model to infer the properties of a population based on observations from a survey. Real-world surveys can have many complexities (e.g., measurement uncertainties, target selection, instrumental effects, data reduction pipeline, detection probability that depends on unobserved properties) that make it impractical to write down the correct likelihood. Instead, ABC relies on: 1) the ability to generate samples from a forward-model for the intrinsic population and survey, and 2) a physically-motivated distance function that quantifies the distance between the actual survey results and the results of a simulated survey. For a sufficiently large number of simulated catalogs and a well-chosen distance function, the ABC posterior estimate converges around the true posterior. Thus, ABC is ideally suited to inferring planet occurrence rates based on transit surveys such as Kepler.

Here we provide a qualitative description of naive ABC and the sequential importance sampling method applied in this study. The occurrence rate of planets within a given

range of sizes and orbital periods is characterized by model and a set of hyperparameters. We apply a model that is a piece-wise constant rate per logarithmic bin in orbital period and planet size. The hyperparameters are simply the occurrence rates for each bin in the 2-d grid. For this study, we chose a period-radius grid with similar period and radius bins: $P = \{0.5, 1, 2, 4, 8, 16, 32, 64, 128, 256, 500\}$ days & $R_p = \{0.5, 0.75, 1, 1.25, 1.5, 1.75, 2, 2.5, 3, 4, 6, 8, 12, 16\}$ R_\oplus . We repeatedly draw planets from this model, simulate observations by the Kepler mission, compute a set of summary statistics (in this case the number of detected planets in each bin) and compare the number of planets (within a certain range of planet sizes and/or orbital periods) that would have been detected in the simulated dataset to the actual number of such planets detected by the Kepler mission. A naive application of ABC would involve drawing hyperparameters from their prior distribution and keeping parameters that resulted in matching the observed number of planets in each bin exactly. While straightforward, this approach is computationally unfeasible for our application.

The implementation of ABC used in this study is Population Monte Carlo, wherein multiple generations of simulated data are created. In each generation, a population of model parameters are used to generate and evaluate multiple simulated catalogs. Simulated catalogs with a distance less than some threshold (“ ϵ ”) are kept and the values of their hyperparameters inform the values of hyperparameters proposed for the following generation. Each set of hyperparameter values is assigned a weight, and sequential importance sampling is used to ensure that the weights properly account for the prior probability distribution at each generation. This sequential importance sampling continues until one of several stopping criteria are met which indicate sufficient convergence has been achieved. For a full description of ABC and the particulars of the ABC-PMC algorithm we use, see Hsu et al. (2018).

While we generally apply the ABC procedure detailed in Hsu et al. (2018), there were a few modifications to account for this study. In this study, each generation of ABC-PMC consists of 100 to 500 “particles” (increased from 50). We found an increased number of particles to be helpful when applying the algorithm to infer several occurrence rates simultaneously, particularly when some of the rates were weakly constrained by the data (see §2.4). Instead of always using the same number of target stars and value of τ (which controls the width of the importance sampler’s proposal distribution), we split the ABC simulation into three steps. For the first 15 generations of each ABC simulation, we create simulated catalogs with only $N_* = 1000$ targets and set $\tau = 1.5$. This accelerates the ABC-PMC algorithm as it “zooms in” on the relevant region of parameter space. For future generations, we set $\tau = 2$ and generate larger simulated

catalogs of $N_* = 10,000$ targets, so as to provide a good importance sampling density for future generations. The ABC-PMC algorithm continues for more generations until satisfying the stopping criteria described in Hsu et al. (2018). In the third step, if the simulation was using less than 200 particles, we run one more generation of ABC using 200 particles drawn using the distance goal (ϵ) of the last generation to provide a larger posterior sample for plotting and computing percentiles.

2.2. Model Improvements

The majority of the physical model in the Exoplanet System Simulator (known as “SysSim”) used in this study has remained the same as in our previous application of ABC to estimate the occurrence rates of planet candidates around FGK stars based on the Q1-Q16 Kepler catalogs in Hsu et al. (2018) (see Section 3). Below we summarize several improvements made for this study.

2.2.1. Stellar Properties

The second Gaia data release (DR2) (Gaia Collaboration et al. 2018) provides significantly improved stellar parameters for the overwhelming majority of the Kepler target stars. Improvements in stellar radii determinations result in more accurate planet radii (and more accurate assigning of planet candidates to their appropriate radii bins). For this study, we adopt the planet-star radius ratio reported in Kepler DR25 (Thompson et al. 2018), but replace the stellar radius with results from Gaia DR2 (Andrae et al. 2018). An initial cross-match was performed using <https://github.com/megbedell/gaia-kepler.fun>. We filter this target list further to remove poor planet search targets, as described in §3.1. Note that we do not use the stellar radii derived by Berger et al. (2018), as that catalog makes use of additional observations (e.g., spectroscopy, asteroseismology) that are not available for all stars. While using additional observational constraints likely improves the precision for individual stars, using such an inhomogeneous set of stellar parameters risks biasing our results.

Additionally, Gaia’s precise parallax measurements allow for more accurate identification of main-sequence stars based on their position in the color-luminosity diagram. We use this information (in place of estimates based on $\log g$) to define a clean sample of FGK main-sequence target stars. Finally, we make use of Gaia’s astrometric information to identify targets likely to be multiple star systems with stars of similar masses/luminosities. The details of our target selection are described in §3.1. This results in a total of 79,935 Kepler targets for which the Kepler DR25 pipeline and robovetter identified 2,524 planet candidates with $P = 0.5 - 500$ d and $R_p = 0.5 - 16R_\oplus$.

2.2.2. Incorporating Kepler DR 25 data products

Planet Catalog: This study makes use of the Kepler DR 25 planet catalog and its associated data products (Thompson et al. 2018). This represents a substantial improvement over the Q1-16 catalog used in Hsu et al. (2018). The DR25 catalog makes use of the light curves from the full Kepler prime mission and incorporates several improvements to the data reduction, planet search, and vetting algorithms. Even more importantly, DR25 was the first Kepler catalog to be generated using a uniform data reduction, planet search and vetting process. For planet occurrence studies, uniformity of processing is particularly important, as it enables statistical modeling of the detection process.

Planet Detection Efficiency: When computing occurrence rates, it is important to use an accurate detection efficiency model for the probability that a planet with known properties is included in the result catalog of planet candidates. Hsu et al. (2018) used a detection efficiency model from Christiansen et al. (2015) that was calibrated to transit injection tests performed using a previous pipeline. In this study, we update the planet detection efficiency model based on transit injection tests based on the DR 25 pipeline Christiansen (2017). Initially, we adopted the detection probability for a transiting planet as a function of the expected effective signal-to-noise ratio (SNR),

$$p_{\text{det,DR25}}(\text{SNR}) = c \times \gamma(\alpha, \beta \times \text{SNR}) / \Gamma(\alpha), \quad (1)$$

where γ is the incomplete gamma function, Γ is the gamma function, $\alpha = 30.87$, $\beta = 0.271$, and $c = 0.94$, based on §5 of Christiansen (2017). This expression models the probability that a transiting planet is detected by the pipeline as a threshold crossing event, but does not attempt to model the probability that a threshold crossing event is promoted to a Kepler Object of Interest or a planet candidate. Most previous studies have simply assumed that all true planets that are identified as threshold crossing events survive the vetting process. Mulders et al. (2018) presented a first attempt to estimate the impact of the vetting process. In this study, we consider three models for the combined planet detection process (i.e., being identified as a threshold crossing event by the pipeline and labeled as a planet candidate by the robovetter). First, we adopt $p_{\text{det,DR25}}$ from Eqn. 1 and assume perfect vetting (i.e., $p_{\text{vet}} = 1$). Second, we adopt the product of $p_{\text{det,DR25}}$ and the Mulders et al. (2018) model for vetting efficiency,

$$p_{\text{vet,Mulders}}(R_p, P) = c R_p^{a_R} \begin{cases} (P/P_{\text{break}})^{a_P}, & \text{if } P < P_{\text{break}} \\ (P/P_{\text{break}})^{b_P}, & \text{otherwise} \end{cases}, \quad (2)$$

where R_p is planet radius (in R_\oplus), P is the orbital period (in days), $c = 0.68$, $a_R = 0.19$, $P_{\text{break}} = 53$, $a_P = -0.07$ and $b_P = -0.39$. Note that this model implies a vetting efficiency that does not explicitly depend on the effective transit SNR, but rather has only an indirect dependence via the planet size

and orbital period. Since the power of the vetting process depends primarily on the ability of the robovetter to features in the shape of the light curve, it is likely that the vetting efficiency indeed depends more directly on the effective measurement noise for the target star. Another concern with this model is that it assumes the probability of a planet being detected by the pipeline and a planet passing vetting are uncorrelated. Since both the pipeline detection efficiency and vetting efficiency depend on the transit light curve (and thus key properties such as the transit signal to noise and the number of transits observed), assuming that these are independent seems unwise. These (as well as results described in §2.5) motivated us to create a new model of the planet detection and vetting process.

For the third model, we derive a combined model for the probability of a transiting planet being detected and labeled as a planet candidate by the robovetter using the pixel-level transit injection tests (Christiansen 2017) and the associated robovetter results (Coughlin 2017).

$$p_{\text{det}\&\text{vet}}(\text{SNR}, N_{tr}) = c_{N_{tr}} \times \gamma(\alpha_{N_{tr}}, \beta_{N_{tr}} \times \text{SNR}) / \Gamma(\alpha_{N_{tr}}), \quad (3)$$

where N_{tr} is the number of “valid” transits observed by Kepler and values for α , β , and c are given in Table 1. (The Kepler photometric reduction pipeline assigned weights to each flux measurement, so as to deweight observations that may be spurious for a variety of reasons (e.g., measurement near a data gap or anomaly). Following Christiansen (2017), a transit is labeled as “valid” if the central flux measurement during the transit has a weight greater than 0.5.)

We follow the general procedure recommended in Christiansen (2017) for fitting a probability as a function of the effective SNR. However, we only consider an injected transit to have been detected if it also is labeled as a planet candidate by the robovetter. The choice of N_{tr} as the second model parameter was motivated by the observation that the vetting efficiency decreases for planets with longer orbital periods and thus smaller N_{tr} . Theoretically, we expect that the dispersion in the measured SNR will depend directly on the number of transits that are contributing to the candidate and only indirectly on orbital period. For example, if two planets have a similar orbital period, but fewer transits of one planet were observed (e.g., due to falling on the CCD module that died early in the Kepler mission), then the distribution of effective SNR would be broader for the planet with fewer observed transits. We adopt this as our baseline model and compare the results using these three models for the combined planet detection process in §4.1.

1 – σ Depth Function: Each of the above planet detection models depends on computing the expected effective SNR. In Hsu et al. (2018), we used the product of the transit depth times the transit duration times the square root of the number of transits for the “signal”. For “noise”, we took the mission

average of the 4.5 hour duration combined differential photometric precision (CDPP) for each target star and assumed that the fractional noise scaled with one over the square root of the number of measurements.

In this study, we make use of a new data product provided by DR25, the “1- σ depth function” (OSDF), which describes the transit depth that would result in a SNR of unity for a given target star, orbital period, and transit duration, after averaging over the epoch of transit (Burke & Catanzarite 2017a). Thus, the expected effective SNR becomes simply the transit depth divided by the OSDF for the target star interpolated to the orbital period and appropriate transit duration. The CDPP is effectively an averaged version of the OSDF that assumes a specific transit duration and averages over orbital period. Thus, we expect the OSDF to be a more accurate measure of the effective noise as it accounts for how the photometric noise deviates from white noise. For planets with a modest number of transits, the SNR can be affected by whether they occur at times with more or less noise than typical. This is particularly significant for planets with orbital periods greater than 90 days, since there is a smaller number of transits and the number of transits observed with one CCD module may differ significantly from the number of transits observed with another CCD module.

The original Kepler DR25 OSDFs are defined for every star, all 15 pulse durations that were searched by the pipeline, and for each of a large ($\sim 10^4$) number of orbital periods (Burke & Catanzarite 2017a). In order to reduce the memory requirements, we downsample these through linear interpolation to a common period grid for all stars of 1000 logarithmically-spaced periods from 0.49 to 700 days, which captures the vast majority of the information in these OSDFs.¹ Though the amount of memory required for SysSim to use OSDFs is much higher than before, its run-time performance did not increase significantly.

When evaluating the noise of a particular planet, we typically use bi-linear interpolation between the period and duration. However, OSDFs are not defined for all periods and durations because the Kepler Transit Search pipeline did not search every combination of period and duration. When the simulated planet’s duration was shorter than the shortest duration searched (and available in OSDF), we assume that the SNR was diluted by the ratio of the searched duration to the actual duration since the search pipeline effectively adds noise to such short duration transits.

When the simulation planet’s duration was longer than the longest duration searched at that period, we adopt the noise

¹ The OSDFs for each star are available from the Kepler mission at https://exoplanetarchive.ipac.caltech.edu/docs/Kepler_completeness_reliability.html. Our downsampled versions are in a more convenient format and available on GitHub.

Table 1. Parameters for $p_{\text{det\&vet}}$

N_{tr}	α	β	c
3	33.3884	0.264472	0.699093
4	32.8860	0.269577	0.768366
5	31.5196	0.282741	0.833673
6	30.9919	0.286979	0.859865
7-9	30.1906	0.294688	0.875042
10-18	31.6342	0.279425	0.886144
19-36	32.6448	0.268898	0.889724
≥ 37	27.8185	0.32432	0.945075

NOTE—We model the probability that a transiting planet is detected by the Kepler DR25 pipeline and labeled as a planet candidate by the robovetter with Eqn. 3 and these parameters. For large SNR the detection/vetting probability asymptotes at c . The detection probability increases most rapidly at an expected effective SNR of $(\alpha - 1)\beta$. The rate of increase in the detection probability is characterized by α/β^2 . For comparison, (Christiansen 2017) reported a fit to the DR25 detection efficiency (not including vetting) of $\alpha = 30.87$, $\beta = 0.271$, and $c = 0.94$. $p_{\text{det\&vet}}$ and Eqn. 1 are similar for large N_{tr} , but deviate significantly for small N_{tr} .

of the longest duration searched. The SNR is reduced due to the signal only accumulating for the duration searched rather than the true duration.

The “timeout” corrections for which stars and durations were searched in DR25 have not been incorporated to our model. This affects only a small fraction of our target stars, as discussed in §4.3.

Window Function: For the Kepler pipeline to detect a planet candidate, there must be good data for at least three transits. This becomes non-trivial for long period planets and/or stars not observed for the full mission duration. Following (Burke et al. 2015), Hsu et al. (2018) adopted a binomial model for the probability that at least three transits were observed, based the expected number of transits if there were no data gaps and the target-specific duty cycle.

In this study, we make use of the DR25 Window Function data products which tabulate the probability of detecting at least three transits as a function of orbital period (Burke & Catanzarite 2017a). As with OSDFs, the provided Kepler DR25 Window Functions are a function of star, duration, and period. These were downsampled to 1000 linearly-spaced periods from 0.5 to 700 days using linear interpola-

tion.² For a simulated planet, SysSim uses bilinear interpolation on these window functions to determine the value of the window function for each simulated planet. As in Hsu et al. (2018), the SNR-detection probability is multiplied by this value to return the final probability of detecting a planet.

Since window functions are identical for targets that were observed in the same sequence of quarters, we identify the 100 most common window functions for targets that were observed for at least 4 quarters as part of the Exoplanet target list (determined by requiring "EX" to be in the Investigation ID as recorded on MAST (archive.stsci.edu/kepler)). These 100 window functions provide an exact match for practically all of our targets. Any targets for which the exact window function was not available were assigned a randomly drawn window function.

Minor improvements affecting detection efficiency: We also incorporate several minor model improvements when calculating the effective signal to noise. For example, Hsu et al. (2018) ignored limb-darkening. In this study, we ac-

² The original versions are also at https://exoplanetarchive.ipac.caltech.edu/docs/Kepler_completeness_reliability.html and our downsampled versions are available on GitHub.

count for limb-darkening when computing the transit depth, using the limb darkening parameters from the Kepler DR 25 stellar catalog, the same values as used for the Kepler pipeline run that produced the DR25 planet candidate catalog. Additionally, we account for dilution of transit depth due to contamination as tabulated in the Kepler Input Catalog. Finally, we have improved the calculation of the transit duration, by using Eqn. 15 of [Kipping \(2010\)](#), so as to avoid making the small angle approximation.

2.3. Sky-averaged detection probabilities using CORBITS

In order to improve the wall-time efficiency of our ABC calculation, we have implemented a probabilistic simulated catalog approach. Previously, when simulating observations to determine the detection probability of each simulated planet, we assigned a geometric transit probability of either zero or unity depending on whether the planet would appear to transit for a single observer orientation. In this study, we assign each potentially detectable planet a weight proportional to its transit detection probability marginalized over all possible observer orientations. The geometric transit probability for each planet is multiplied by a transit detection efficiency that is marginalized over all impact parameters (that result in a transit) to give the total detection probability. For a single planet, the sky-averaged geometric transit probability for each planet is $R_*/[a(1-e^2)]$, where R_* is the stellar radius, a is the semi-major axis and e is the orbital eccentricity. For stars with multiple planets, SysSim calculates the sky-averaged geometric transit probability for each planet, as well as each pair of planets and each number of transiting planets in the system. The CORBITS package ([Brakensiek & Ragozzine 2016](#)) makes this computationally practical by using semi-analytic methods to determine the transit probability of each combination of planets associated with a given planetary system.³ Using the sky-averaged detection probability instead of the detection probability for a single viewing geometry reduces the number of simulated planetary systems needed to accurately infer planet occurrence rates. As part of our model and algorithm verification, we determined that the number of planetary systems drawn could be reduced by a factor of $\simeq 8$ relative to the number of target stars without significantly affecting the accuracy of the inferred occurrence rates. This reduction offsets the overhead from CORBITS, which increases the calculation time from single observer by a factor of $\simeq 6$. Therefore, the overall reduction is about one-third off the previous calculation time. While this provides

³ CORBITS requires that orbits not “cross”, i.e., if $a_1 < a_2$, then it requires that $a_1 \times (1+e_1) < a_2 \times (1-e_2)$. Physically, such configurations are unlikely due to long-term orbital stability. Therefore, when multiple planets are assigned to a single star, we reject configurations that result in crossing orbits and redraw until a configuration without crossing orbits is created (up to a maximum of 20 times).

only a modest performance improvement for this study, we anticipate that the sky-averaged observing geometry mode will be particularly valuable for future studies that investigate the occurrence rate of systems with multiple transiting planets.

In [Hsu et al. \(2018\)](#), the distance function used by ABC was simply the absolute value of the difference in the ratios of detected planets to stars surveyed for the simulated and observed planet catalogs. Since this study averages over viewing geometries, simply summing the detection probabilities would result in the expected number of planet detections which is not directly comparable with the observed number of planets of the actual Kepler data. The expected number of planet detections has a smaller variance than the actual number of planet detections. Therefore, after calculating the detection probabilities for each planet in a simulated catalog, we label each planet as either detected or not-detected based on a Bernoulli draw with success probability equal to each planet’s total detection probability.

2.4. Inferring multiple occurrence rates simultaneously

In [Hsu et al. \(2018\)](#), we inferred the occurrence rate for each “bin” in period and radius independently of other bins. Orbital periods are measured so precisely that there is effectively no ambiguity about which period bin a planet should be assigned to. In principle, three effects could cause a planet to be assigned to a different bin than it would be if its properties were known perfectly. First, measurement errors cause the observed planet-star radius ratio to differ from its true value. Fortunately, this happens for only a small fraction of planets. Indeed, [Hsu et al. \(2018\)](#) found that this effect did not result in significant correlation between neighboring planet radii bins. Second, uncertainties in the stellar properties cause the measured planet radius to differ from the true planet radius, even if the planet-star radius ratio were known precisely. Nearly all previously published studies, including [Hsu et al. \(2018\)](#), have neglected this effect. Shabram et al. (2019, submitted) showed that uncertainties in host star radii could have a significant effect on planet occurrence rates. In this study, we infer multiple occurrence rates simultaneously, so as to account for this effect. A third source of uncertainty (unrecognized contamination) is discussed in 4.3, but is not modeled in this study.

Once Gaia provided accurate parallaxes for most Kepler target stars ([Gaia Collaboration et al. 2018](#)), accurate stellar radii and uncertainties were derived for those targets ([Andrae et al. 2018](#)). This makes it feasible to accurately model the effects of uncertainty in stellar radii on planet occurrence rates. Since planet radii are proportional to the host star radius, uncertainty in host star radius directly translates into uncertainty in the planet radius. Even with Gaia DR2 parallaxes, the uncertainty in stellar radius can result in a planet being assigned

to the wrong radius bin. For each planet we simulate, the true transit depth is based on the true planet radius and the stellar radius from Gaia (Andrae et al. 2018). We draw an assumed stellar radius from an equal mixture of two half-normal distributions with median equal to the Gaia best-fit radius and use Gaia’s upper and lower uncertainties for the standard deviations of the half-normals (Andrae et al. 2018). If the uncertainty in stellar radius (in either direction) is less than 6% the value of the radius, then we increase that uncertainty to 6% the stellar radius (based on the distribution of stellar radius uncertainties in Berger et al. (2018)). Then, we draw the observed transit depth centered on the true transit depth with a width based on its SNR and the diagonal noise model of Price & Rogers (2014) that accounts for finite integration time. Next, we compute the “observed” planet radius from the observed planet-star radius ratio and the assumed stellar radius. In most cases, the observed planet radius results in the planet being assigned to the same bin as it would be if its radius were known precisely. However, sometimes, the observed planet radius results in the planet being assigned to a neighboring bin containing slightly larger or smaller planets. If one were to include the uncertainty in stellar properties, but only modeled planets drawn from a single bin, then the inferred planet occurrence rate would be biased to be larger than the true rate, since simulated planets can “leak” beyond the boundaries of the radius bin. The magnitude of the effect depends on the size of the bin in radius relative to the size of uncertainties in stellar properties and on the differences between occurrence rates in neighboring bins. In tests, we found that this effect could lead to occurrence rates being inflated by $\sim 20\%$ of the measured rate (for bins focusing on small planets with a width of $0.25 R_{\oplus}$), if each bin were analyzed individually, rather than in a group.

2.4.1. Model Parameterization

Fortunately, our ABC approach naturally accounts for this effect, as long as we simultaneously model the occurrence rate of planets in each size bin. When performing inference with occurrence rates for multiple radius bins, we performed calculations using two sets of priors, each with their own model parameterization. First, we assign each bin in period and radius its own occurrence rate, with a uniform prior. This has the advantage that the prior for any individual bin is easy to understand. However, it has the disadvantage that the total number of planets within a range of orbital periods could be larger than plausible if one considers long-term orbital stability. Second, we allow each period bin to have a total occurrence rate with uniform prior, and assign a fraction of those planets to each radius bin. This prior has the advantage that the rate of planets summed over all sizes is constrained. However, the Dirichlet prior over the fractions in each radius bin makes it more difficult to visualize the prior.

For most periods and sizes, the choice of prior did not have a significant impact on the posterior for occurrence rates. The differences were more noticeable for small, long-period planets. Therefore, we will report results for both choices of prior in the η_{\oplus} regime.

The individual occurrence rates $f_{i,j}$ are used for the entire period-radius grid considered. We adopt a uniform prior for $f_{i,j}$ over $[0, f_{\max,i,j}]$. The upper limit $f_{\max,i,j} = C \times \log_2(P_{\max,j}/(2P_{\min,j})) \times \log_2(R_{\max,i}/(2R_{\min,i}))$, where we set $C = 2$. This choice is small enough that proposals with more than 3 planets per factor of 2 in period are extremely rare, consistent with expectations based on long-term orbital stability. Once computations are finished, we verified that the inferred posterior distributions were not being truncated by the prior’s upper limit.

When deriving our best estimate of planet occurrence rates in the η_{\oplus} regime, we will adopt the second model parameterization. For each bin in orbital period (indexed by j), we infer: 1) $f_{\text{tot},j}$, the total occurrence rate for all planets within the range of orbital periods and the full range of planet sizes being considered, and 2) a vector $f_{\text{rel},i,j}$: the fraction of planets in the j th orbital period bin that have sizes falling within the range of the i th radius bin. Thus, the occurrence rate for planets in the i th radius bin and j th period bin is given by $f_{i,j} = f_{\text{tot},j} f_{\text{rel},i,j}$. We adopt a uniform prior for $f_{\text{tot},j}$ over $[0, f_{\max,\text{tot},j}]$. The upper limit $f_{\max,\text{tot},j} = 3 \times \log_2(P_{\max,j}/(2P_{\min,j}))$ is motivated by long-term orbital stability, as it is rare for 3 planets to have orbital periods within a factor of 2 of each other (though a few cases are known to exist for very small planets). For each $f_{\text{rel},i,j}$ (a vector with j fixed), we adopt a Dirichlet prior with concentration parameters proportional to $\log(R_{\max,i}/R_{\min,i})$. The smallest concentration parameter is set to unity. The Dirichlet prior ensures that $\sum_i f_{\text{rel},i,j} = 1$ to within numerical precision.

2.4.2. Distance Function

Now that we allow for uncertainty in stellar properties, we revisit the choice of distance function for using with ABC. We performed tests on simulated data to verify our algorithms and to compare the performance of multiple distance functions. Simply summing the absolute value of the difference in the ratios of detected planets to stars surveyed for the simulated and observed planet catalogs often resulted in an ABC posterior with highly disparate widths for different bins. Since bins with a greater number of observed planets have a greater contribution to the total distance, ABC would result in precise occurrence rates for well-populated bins, but much less precise estimates of occurrence rates for bins with low rates of planet candidates. For many scientific purposes, one would prefer a similar fractional error in occurrence rates for all bins, rather than a similar absolute error in occurrence rates for all bins. Therefore, we choose a new distance func-

tion that weights the absolute value of the difference in the ratio of detected planets to targets for each bin by the square root of the sum of the ratio of detected planets to targets for the simulated and observed planet catalogs for that bin. This modified Canberra distance is given by

$$\rho(s_{\text{obs},k}, s_k^*) = \sum_k \frac{|s_{\text{obs},k} - s_k^*|}{\sqrt{s_{\text{obs},k} + s_k^*}}, \quad (4)$$

where, for each k th period-radius bin, $s_{\text{obs},k}$ is the ratio of number of planet candidates detected by Kepler to the number of target stars searched and s_k^* is ratio of the number of planets detected to target stars in the simulated catalog. We found that this distance function allows ABC to converge more rapidly when inferring occurrence rates for multiple bins simultaneously. We tested that this algorithm accurately simulates both the number of planets detected and the dispersion in the number of planets detected for the simulated catalogs. We also tested that the Canberra distance function accurately estimates the true planet occurrence rate and its uncertainty (by comparing to simulations that do not make use of sky-averaged detection probabilities; see §2.5 and Figure 1).

2.4.3. Importance Sampler Proposal Distribution

Initially, we attempted to apply the sequential importance sampler in the ABC-PMC algorithm using a multivariate Gaussian for the proposal distribution, as described in [Beaumont et al. \(2008\)](#) and [Hsu et al. \(2018\)](#). However, this proved computationally prohibitive. For example, a proposal of a negative value for any one bin would result in rejecting the entire proposal; when considering several bins that have small occurrence rates, such proposals are common. In order to make the ABC-PMC algorithm practical, we experimented with a variety of replacement proposal distributions. Eventually, we settled on using a Beta distribution for the proposal for both parameterizations. When using independent priors for each $f_{i,j}$, the ABC-PMC algorithm uses a Beta proposal distribution for each $f_{i,j}$. When using a Dirichlet prior for the relative occurrence rates within a given period bin, the ABC-PMC algorithm using a Beta proposal for $f_{\text{tot},j}$ and each $f_{\text{rel},i,j}/f_{\text{max,tot},j}$. After each proposal, the initially proposed values for the relative rates were rescaled according to $f_{\text{rel},i,j} \leftarrow f_{\text{rel},i,j} / \sum_i f_{\text{rel},i,j}$, so that the rescaled rates sum to unity. We validated the algorithm on simulated data sets and found that this dramatically improved the computational efficiency.

2.5. Verification and Validation

Before applying our improved model and ABC algorithm to actual Kepler catalogs, we performed extensive tests to validate and verify the model, the algorithms, and our implementations.

Figure 1 shows a comparison of results using either the sky-averaging mode (described in §2.3) or the single observing geometry mode for one particular bin (orbital periods of 8-16 days and planet sizes of $1.25\text{-}1.5R_{\oplus}$) where the "true" catalog is set to $f = 3\%$. The blue (orange) points show the median planet occurrence rate inferred for this bin using a single observing geometry (sky-averaged viewing geometry) and the vertical error bars indicate the 68.3% credible region. The horizontal axis indicates the number of occurrence rates inferred simultaneously. For any single simulated catalog, the number of observed planets is likely greater (or less) than the expected number of observed planets, leading to the posterior median rate being larger (or smaller) than the true rate ($f = 3\%$). We performed several simulations to verify that the median posterior rate from multiple runs was distributed about the true value. Figure 1 shows the results of multiple analyses for a single catalog demonstrating that we recover a posterior median close to the true value.

First, we will focus on results for three bins. Note that Sys-Sim yields very similar results, regardless of whether using a single observing geometry (blue) or when using averaging over all viewing geometries (orange). As expected, including stellar radii uncertainties (green) results in an increased width of posterior distribution relative to an analysis which assumes stellar radii are known perfectly (orange).

Next, we compare results as a function of the number of occurrence rates inferred simultaneously. Each method (single observing geometry or sky-averaged viewing geometries, excluding or including uncertainties in stellar properties) gives statistically indistinguishable results for the median occurrence rate, as long as the number of model parameters being inferred simultaneously does not exceed seven. When analyzing three or five radius bins simultaneously, the posterior widths are very similar. In either case, the posterior width is observed to increase modestly when the model accounts for uncertainties in stellar radii. When analyzing nine radius bins simultaneously, the posterior width has increased noticeably. This behavior is typical of the sequential importance sampler used by the ABC-PMC algorithm. When performing inference on nine parameters simultaneously, it becomes less likely that the proposed values for all nine parameters will result in a precise match for the number of observed planets in all nine bins. As a result, the computational time required for ABC-PMC to achieve a given distance increases significantly. In practice, the final distance achieved by the ABC-PMC algorithm begins to increase substantially as the number of dimensions increases beyond seven, resulting in an increased width of the ABC-posterior. Thus, we must balance the desire to minimize bias with the desire to minimize unnecessary increase in posterior width due to computational limitations. Minimizing bias leads us to perform inference on at least three bins simultaneously. Avoiding an unnecessary

increase in posterior width limits us to performing inference on ≤ 7 bins simultaneously.

Next, we performed several tests to further fine tune the choice of how many occurrence rates to infer simultaneously. When inferring occurrence rates for multiple radius bins simultaneously, we find that only the top and bottom bins display noticeable bias. This is expected since the model effectively assumes that there are no detectable planets with radius greater than the upper limit of the top bin or less than the lower limit of the bottom bin. Since the bias is proportional to the difference between the true and assumed rate of such planets, it is maximized when the assumed rate is zero. When inferring occurrence rates for just three bins simultaneously, one could worry that the estimated rates for both edge bins will be overestimated and this could have an indirect effect on the estimated rate for the central bin. In practice, the bias for the central bin is a second-order effect and significantly smaller than the other uncertainties. A related effect occurs when two bins (neighboring in radii) have a large difference in occurrence rate. If the “leaking” of planets out-of and in-to the radius bin in question is not symmetric, then the impact of stellar uncertainties is amplified compared to other sets of bins where the occurrence rate is similar above and below the bin in question. This demonstrates that it is important to model the uncertainties in stellar radii and to simultaneously infer the planet occurrence rates when estimating planet occurrence rates for a wide range of planet radii and orbital periods.

Based on the above tests, we settled on reporting results using simulations that simultaneously infer planet occurrence rates for 5 (or 7) radius bins, reporting the results for the interior 3 (or 5) radius bins. (One exception is that we also report the occurrence rate for our largest bin, 12–16 R_{\oplus} , as explained below.) In order to span the full range of planet radii and to avoid significantly overestimating the ABC-posterior width, we perform multiple simulations, each using 5 to 7 radius bins. The specific bin boundaries chosen for the subsets were: $R_p = \{0.25, 0.5, 0.75, 1, 1.25, 1.5\}, \{0.5, 0.75, 1, 1.25, 1.5, 1.75, 2, 2.5\}, \{1, 1.25, 1.5, 1.75, 2, 2.5\}, \{1, 2, 2.5, 3, 4, 6\}, \{3, 4, 6, 8, 12, 16\} R_{\oplus}$ for each period range.

Formally, one should be cautious in using results from an “edge bin”. Therefore, for each subset we throw out the two edge bins and take estimates for only interior bins from each subset. In the case of bins which are interior to multiple subsets, we combine the final populations produced by the separate runs on each subset to produce the occurrence rate estimates. The one edge bin which we do not throw out is the 12–16 R_{\oplus} bin. Even though the 12–16 R_{\oplus} bin is an edge, the rate of planets larger than 16 R_{\oplus} is so small that there is no practical impact on the measured occurrence rates for 12–16 R_{\oplus} planets. While we include occurrence rates for 0.25–0.5 R_{\oplus} planets in our model calculations, we do so primarily so as

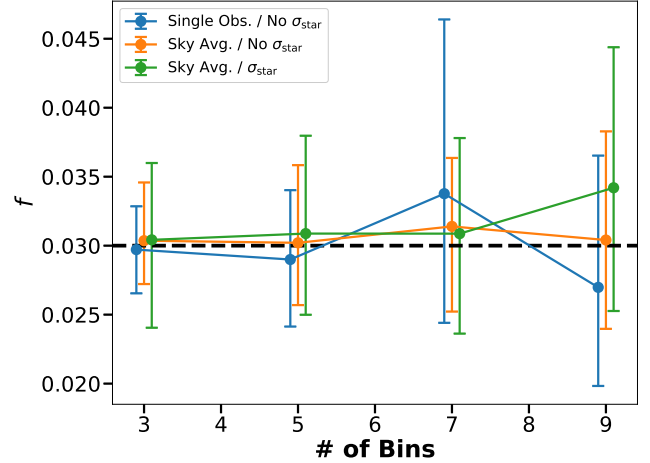


Figure 1. Occurrence rate estimates for the 8–16d period, 1.25–1.5 R_{\oplus} planet radius bin using a simulated “true” catalog. This catalog was created with the rates $f = \{0.07, 0.06, 0.05, 0.04, 0.03, 0.02, 0.01, 0.005, 0.0025\}$ for the bins $R_p = \{0.25–0.5, 0.5–0.75, 0.75–1, 1–1.25, 1.25–1.5, 1.5–1.75, 1.75–2, 2–3, 3–4\} R_{\oplus}$. For each run, 1, 2, 3, and 4 neighboring radii bins on each side of the the 8–16d period, 1.25–1.5 R_{\oplus} planet radius bin are simultaneously fit for a total number of bins of 3, 5, 7, and 9 bins. In the case of 9 bins, the full range of bins used in the creation of the catalog are fit, while for runs with fewer bins the outer two bins were consecutively removed until the appropriate number of bins is reached. The dashed black line indicates the true rate for the 1.25–1.5 R_{\oplus} bin ($f = 3\%$). Estimates based on a single observing geometry (blue) and sky-averaged viewing geometries (orange) are consistent. Excluding (orange) or including (green) stellar uncertainties does not affect the median estimated rate. However, the uncertainty in the estimate of the occurrence rate increases when uncertainties in the stellar radius are included in the model. The median estimated rate does not significantly vary with increasing number of bins, but the width of the ABC-posterior does increase with the number of bins inferred simultaneously.

to ensure that our estimates for 0.5–0.75 R_{\oplus} planets are accurate. Thus, we do not include the inferred rates for 0.25–0.5 R_{\oplus} planets in Figure 2 out of an abundance of caution.

3. APPLICATION TO DR25

3.1. Catalog Selection

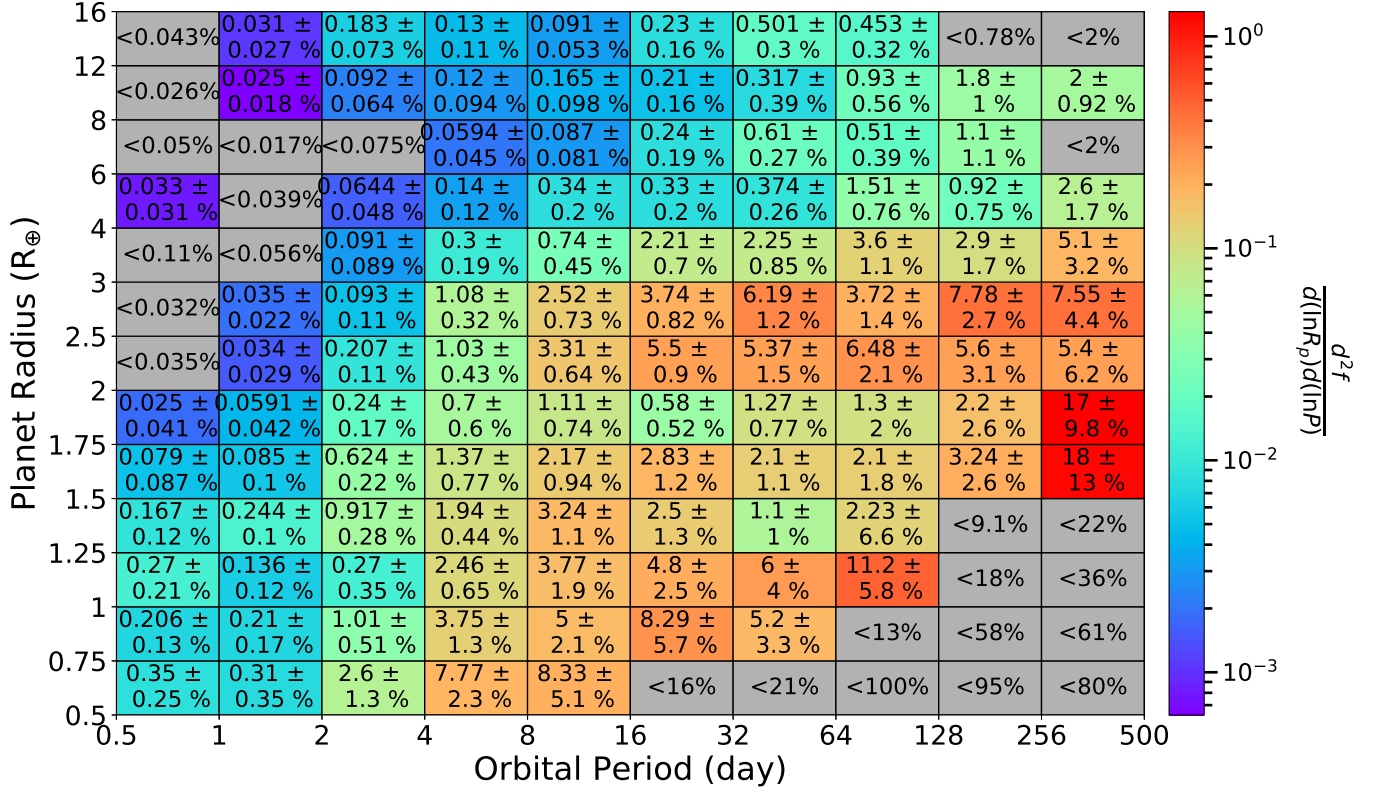
The second Gaia data release (DR2) (Gaia Collaboration et al. 2018) provides significantly improved stellar parameters for the overwhelming majority of the Kepler target stars. Improvements in stellar radii determinations result in more accurate planet radii and more accurate assigning of planet candidates to their appropriate radii bins. Additionally, Gaia’s precise parallax measurements allow for more accurate identification of main-sequence stars based on their position in the color-luminosity diagram. We use this information (in place of estimates of $\log g$) to define a clean sample of FGK main-sequence FGK target stars. Finally, we

make use of Gaia’s astrometric information to identify targets likely to be multiple star systems with stars of similar masses/luminosities.

We construct a catalog of Kepler target stars starting from the Kepler DR25 stellar properties catalog and augmented with data from Gaia DR2 (Gaia Collaboration et al. 2018). The selection criteria used to select Kepler targets likely to be main-sequence FGK stars are as follows (applied in order):

1. **Require that the Kepler magnitude and the Gaia G magnitude are consistent.** We compute the median and standard deviation of the difference in the Kepler magnitude and Gaia G magnitude based on the initial cross-matched catalog based on position. If a target’s Kepler magnitude minus Gaia G magnitude differs from the median by more than 1.5 times the standard deviation, then it is excluded from our cleaned catalog. This filter makes sure that a Kepler target is not erroneously matched to a Gaia target corresponding to a background star.
2. **Require $\text{Gaia GOF_AL} \leq 20$ and Gaia astrometric excess noise ≤ 5 cut.** These criteria indicate a poor astrometric fit. This is often caused by an unresolved astrometric binary star (Evans 2018).
3. **Require Gaia Priam processing flags that indicate the parallax value is strictly positive and both colors are close to the standard locus for main-sequence stars.** This rejects Kepler targets which are unlikely FGK main sequence stars or are so distant that Gaia does not have a good parallax measurement and the stellar radius will be highly uncertain.
4. **Require Gaia parallax error is less than 10% the parallax value.** This excludes some faint/distant Kepler targets for which accurate stellar radii would not be available. Of all our target selection criteria based on data quality this results in the largest decrease in the number of target stars and planet candidates. In principle, future observations (e.g., improved Gaia data releases) could increase the number of stars with accurate stellar properties, perhaps allowing for more precise planet occurrence rate measurements. However, for FGK main-sequence stars, this criterion only excludes distant and hence faint targets for which Kepler does not have significant sensitivity to small planets in the habitable zone. Therefore, we expect that even future Gaia data releases and other follow-up observations to improve stellar characterization will not lead to significant improvements in the constraints on the occurrence rate of small planets in or near the habitable zone of main-sequence FGK stars.
5. **Require that Kepler DR 25 provide a valid Kepler stellar mass, data span, duty cycle, and limb darkening coefficients, and that Gaia’s Apsis module provide a valid stellar radius based on Gaia data** (Andrae et al. 2018).
6. **Require that the Kepler target was observed for > 4 quarters and must have been on the Exoplanet target list for at least one quarter.** These criteria exclude targets that were observed by Kepler for purposes other than the exoplanet search, as these are unlikely to be FGK main sequence stars. A small number of stars that were part of the exoplanet search will also be excluded if they were only observed for ≤ 4 quarters. Kepler does not have significant sensitivity to small planets in the habitable zone of such FGK stars.
7. **Require the target to have a color $0.5 \leq B_p - R_p \leq 1.7$ from Gaia photometry.** This color cut results in selecting FGK stars and is more precise than using the temperature from the Kepler Input Catalog and more uniform than using temperatures from the DR25 stellar catalog.
8. **Require the target star to have a luminosity, $L \leq 1.75L_{MS}(B_p - R_p)$, where $L_{MS}(x) = 2.62 - 3.74x + 0.962x^2$ represents the luminosity of a main-sequence star for a given $B_p - R_p$ color.** To compute $L_{MS}(B_p - R_p)$ we fit a quadratic function to the observed values of L as a function of $B_p - R_p$ for our Kepler targets. We reject those targets whose observed L deviates from L_{MS} by more than 75% and refit the model to the remaining targets. We iterate this process six times before converging on our final model for the main-sequence luminosity L_{MS} . This rejects targets that are significantly above the main sequence, either due to stellar evolution (primarily for F stars) or due to a multiple star system where stars other than the primary contribute $>75\%$ of the total flux. While this final criteria likely removes some viable targets for planet hunting (e.g., F stars starting to evolve off the main sequence), it is a small fraction of the total stars searched and Kepler does not have significant sensitivity to small planets near their habitable zone.

The total number of FGK Kepler target stars remaining after these cuts is 79,935. While the number of targets is significantly less than the total number observed by Kepler, a clean sample of target stars is preferable for performing planet occurrence rate studies. In principle, a less restrictive set of cuts might provide a larger stellar sample and provide more precise estimates for occurrence rates of large planets. However, such a strategy is unlikely to be useful for measuring the occurrence rate of small planets near the habitable zone,



The Kepler DR25 pipeline and robovetter identified 2,524 planet candidates associated with these targets with $P = 0.5 - 500$ days and $R_p = 0.5 - 16R_\oplus$. One noticeable change from our previous study is the relatively few planet candidates in the η_\oplus regime. The primary cause for this change is the usage of updated stellar radii from Gaia, which are often larger than the previously determined Kepler stellar radii. This trend tends to boost the inferred planet radii. As a result, the majority of long period, small radius planet candidates shifted to larger radius bins within the period-radius grid once we incorporated Gaia stellar radii. For example, the inferred radius KOI 7016.01 (Jenkins et al. 2015; Mullally et al. 2018, also known as Kepler-452 b) reported in DR25 is $1.06^{+0.2}_{-0.1} R_\oplus$, but incorporating the updated stellar radii from Gaia DR results in the estimated radius increasing to $1.51 R_\oplus$ (with uncertainties increasing proportionally). While the best-estimate for the planetary radius no longer falls within the $1 - 1.25 R_\oplus$

bin, the uncertainty in the radius of such planets results in it contributing to the estimated occurrence rate. In order to explore which η_\oplus regime planet candidates were removed due to our stellar cuts (as opposed to updated stellar radii), we created a separate target list where we relax the two stellar cuts which most significantly reduced the number of stars in our sample: the FGK luminosity cut and the cuts designed to remove suspected binaries. This catalog has a total number of 139,232 target stars, with 3,170 planet candidates within the limits of the period-radius grid. Most significantly, we recover two long-period, small radius planet candidates (associated with targets KIC 5097856 and 5098334) in the $P = 256 - 500$ days, $R_p = 1.25 - 1.5 R_\oplus$ bin. After investigating the properties of these two planet candidates, we determined that the candidates were not in our final catalog because their associated target stars had poor astrometric GOF which suggests that their host star is likely part of an unresolved binary. If true, then the unmodeled flux from the binary companion would be diluting the transit depth, causing the true planet radius to be larger than currently estimated.

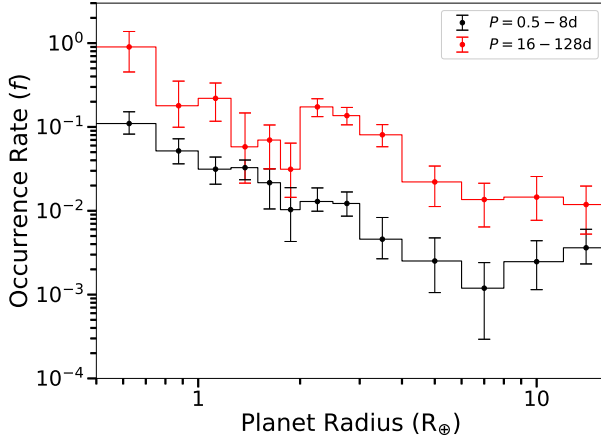


Figure 3. Occurrence rate estimates marginalized over two period ranges: 0.5–8d (black) and 16–128d (red).

We conclude that our process for identifying a clean sample of target stars worked as intended.

3.2. Baseline Planet Occurrence Rates

The values in each bin of Figure 2 state the median of the ABC-posterior for the occurrence rates over the full period-radius grid. Results are tabulated in Table 2. The uncertainties shown are the differences between the median and either the 15.87th or 84.13th percentile (whichever has the larger absolute difference) of the ABC-posterior for each occurrence rate. These rates make use of the combined detection and vetting efficiency (Eqn. 3). For period-radius bins with zero or one observed planet candidates, we report the 84.13th percentile as an upper limit instead of a median rate and uncertainty. For these bins, the posterior distribution is asymmetrical and summarizing the posterior with a point estimate runs a greater risk of misinterpretation. Figure 5 depicts the ABC posterior for the occurrence rate for several long period, small radius bins to demonstrate this asymmetry.

The reported upper limits are conservative in the sense that a full calculation (i.e., inferring rate for all radius bins si-

multaneously within a period range, rather than just 5 at a time) would likely cause a modest reduction in the upper limit. This is because we set a maximum total rate of 3 per factor of 2 in period (as a stability criterion), so a full calculation which adds well-constrained bins at larger radii would reduce the remaining total rate that can be allotted to the bins with only upper limits. Given the occurrence rates inferred, the effect is negligible for most of the parameter space considered. While a few effects (e.g., unmodeled contaminating flux, detection efficiency decreasing for systems with multiple transiting planets, pipeline timeouts) could cause our model to overestimate the detection efficiency for individual planetary systems, each of these affect only a small fraction of stars (see §4.3). Therefore, we expect that any revisions to our upper limits due to these effects would be limited to a few percent. However, for bins with so little constraining data the estimated posterior may be significantly affected by the choice of prior (see §4.2).

In Figure 3, we show the occurrence rate as a function of planet size, marginalized over two separate period ranges, 0.5-8d and 16-128d. The planet radius valley [Fulton et al. \(e.g., 2017\)](#); [Van Eylen et al. \(e.g., 2017\)](#) is apparent for periods of 16-128d, but not for periods less than 8 days. Our use of a cleaned target star sample is designed to reduce effects due to contamination from binary stars, similar to [Teske et al. \(2018\)](#). The depth and width of the valley are expected to depend on orbital period on theoretical grounds ([Lopez & Fortney 2014](#); [Owen & Wu 2017](#); [Gupta & Schlichting 2018](#)). A narrow and deep valley whose location depends on period would appear to be broader and shallower when one marginalizes over a broad range of periods, as in this figure. Therefore, the depth of the valley shown in Figure 3 should be interpreted as a minimum depth when comparing to predictions of model predictions over a narrower range of periods. Comparing the rate of 1.25-1.5 R_{\oplus} planets as a function of orbital periods, we find no evidence that the occurrence rate is decreasing beyond 64 days, as predicted by some models.

Table 2. Inferred Planet Occurrence Rates

Period (days)	Radius (R_{\oplus})	Combined Detection & Vetting Efficiency		No Vetting Efficiency
		0.50– 1.00	0.50– 0.75	
0.50– 1.00	0.75– 1.00	$2.1_{-1.3}^{+1.3} \times 10^{-3}$	$3.5_{-1.9}^{+2.5} \times 10^{-3}$	$2.44_{-1.15}^{+0.85} \times 10^{-3}$
0.50– 1.00	1.00– 1.25	$2.7_{-1.5}^{+2.1} \times 10^{-3}$	$1.97_{-0.94}^{+1.81} \times 10^{-3}$	$2.4_{-1.3}^{+1.2} \times 10^{-3}$
0.50– 1.00	1.25– 1.50	$1.67_{-1.22}^{+0.80} \times 10^{-3}$	$1.48_{-0.93}^{+0.89} \times 10^{-3}$	

Table 2 continued

Table 2 (*continued*)

Period (days)	Radius (R_{\oplus})	Combined Detection &		No Vetting Efficiency
		Vetting	Efficiency	
0.50 – 1.00	1.50 – 1.75	$7.9_{-5.8}^{+8.7} \times 10^{-4}$	$8.5_{-5.4}^{+9.2} \times 10^{-4}$	
0.50 – 1.00	1.75 – 2.00	$2.5_{-1.8}^{+4.1} \times 10^{-4}$	$2.5_{-1.4}^{+2.9} \times 10^{-4}$	
0.50 – 1.00	2.00 – 2.50	$< 3.5 \times 10^{-4}$	$< 6.0 \times 10^{-4}$	
0.50 – 1.00	2.50 – 3.00	$< 3.2 \times 10^{-4}$	$< 3.6 \times 10^{-4}$	
0.50 – 1.00	3.00 – 4.00	$< 1.1 \times 10^{-3}$	$< 5.0 \times 10^{-4}$	
0.50 – 1.00	4.00 – 6.00	$3.3_{-2.6}^{+3.1} \times 10^{-4}$	$2.1_{-1.3}^{+4.9} \times 10^{-4}$	
0.50 – 1.00	6.00 – 8.00	$< 5.0 \times 10^{-4}$	$< 3.7 \times 10^{-4}$	
0.50 – 1.00	8.00 – 12.00	$< 2.6 \times 10^{-4}$	$< 1.7 \times 10^{-4}$	
0.50 – 1.00	12.00 – 16.00	$< 4.3 \times 10^{-4}$	$< 5.5 \times 10^{-4}$	
1.00 – 2.00	0.50 – 0.75	$3.1_{-2.0}^{+3.5} \times 10^{-3}$	$3.46_{-1.95}^{+0.18} \times 10^{-3}$	
1.00 – 2.00	0.75 – 1.00	$2.1_{-1.7}^{+1.4} \times 10^{-3}$	$2.13_{-0.60}^{+0.96} \times 10^{-3}$	
1.00 – 2.00	1.00 – 1.25	$1.36_{-0.84}^{+1.17} \times 10^{-3}$	$1.9_{-1.2}^{+2.0} \times 10^{-3}$	
1.00 – 2.00	1.25 – 1.50	$2.44_{-0.83}^{+1.01} \times 10^{-3}$	$2.23_{-1.00}^{+1.39} \times 10^{-3}$	
1.00 – 2.00	1.50 – 1.75	$8.5_{-6.2}^{+10.5} \times 10^{-4}$	$9.9_{-5.8}^{+9.4} \times 10^{-4}$	
1.00 – 2.00	1.75 – 2.00	$5.9_{-3.7}^{+4.2} \times 10^{-4}$	$5.8_{-3.8}^{+3.4} \times 10^{-4}$	
1.00 – 2.00	2.00 – 2.50	$3.4_{-2.2}^{+2.9} \times 10^{-4}$	$1.9_{-1.3}^{+2.6} \times 10^{-4}$	
1.00 – 2.00	2.50 – 3.00	$3.5_{-2.2}^{+1.3} \times 10^{-4}$	$2.6_{-1.5}^{+5.9} \times 10^{-4}$	
1.00 – 2.00	3.00 – 4.00	$< 5.6 \times 10^{-4}$	$< 4.6 \times 10^{-4}$	
1.00 – 2.00	4.00 – 6.00	$< 3.9 \times 10^{-4}$	$< 3.6 \times 10^{-4}$	
1.00 – 2.00	6.00 – 8.00	$< 1.7 \times 10^{-4}$	$< 2.2 \times 10^{-4}$	
1.00 – 2.00	8.00 – 12.00	$2.5_{-1.7}^{+1.8} \times 10^{-4}$	$2.5_{-1.5}^{+2.2} \times 10^{-4}$	
1.00 – 2.00	12.00 – 16.00	$3.1_{-1.9}^{+2.7} \times 10^{-4}$	$3.8_{-2.5}^{+3.8} \times 10^{-4}$	
2.00 – 4.00	0.50 – 0.75	$2.55_{-0.40}^{+1.28} \times 10^{-2}$	$2.43_{-0.60}^{+0.83} \times 10^{-2}$	
2.00 – 4.00	0.75 – 1.00	$1.01_{-0.37}^{+0.51} \times 10^{-2}$	$1.00_{-0.28}^{+0.35} \times 10^{-2}$	
2.00 – 4.00	1.00 – 1.25	$2.7_{-1.8}^{+3.5} \times 10^{-3}$	$2.4_{-1.4}^{+1.3} \times 10^{-3}$	
2.00 – 4.00	1.25 – 1.50	$9.2_{-2.8}^{+2.5} \times 10^{-3}$	$8.6_{-2.4}^{+2.3} \times 10^{-3}$	
2.00 – 4.00	1.50 – 1.75	$6.2_{-2.2}^{+2.0} \times 10^{-3}$	$6.4_{-2.2}^{+1.9} \times 10^{-3}$	
2.00 – 4.00	1.75 – 2.00	$2.4_{-1.2}^{+1.7} \times 10^{-3}$	$2.4_{-1.6}^{+1.7} \times 10^{-3}$	
2.00 – 4.00	2.00 – 2.50	$2.07_{-0.79}^{+1.14} \times 10^{-3}$	$2.5_{-1.1}^{+1.1} \times 10^{-3}$	
2.00 – 4.00	2.50 – 3.00	$9.3_{-6.5}^{+10.7} \times 10^{-4}$	$9.3_{-5.6}^{+8.1} \times 10^{-4}$	
2.00 – 4.00	3.00 – 4.00	$9.1_{-2.8}^{+8.9} \times 10^{-4}$	$1.07_{-0.31}^{+0.67} \times 10^{-3}$	
2.00 – 4.00	4.00 – 6.00	$6.4_{-3.4}^{+4.8} \times 10^{-4}$	$6.4_{-3.3}^{+4.7} \times 10^{-4}$	
2.00 – 4.00	6.00 – 8.00	$< 7.5 \times 10^{-4}$	$< 4.2 \times 10^{-4}$	
2.00 – 4.00	8.00 – 12.00	$9.2_{-4.2}^{+6.4} \times 10^{-4}$	$8.5_{-5.1}^{+6.0} \times 10^{-4}$	
2.00 – 4.00	12.00 – 16.00	$1.83_{-0.58}^{+0.73} \times 10^{-3}$	$1.96_{-0.74}^{+1.10} \times 10^{-3}$	
4.00 – 8.00	0.50 – 0.75	$7.8_{-2.0}^{+2.3} \times 10^{-2}$	$7.0_{-1.8}^{+2.6} \times 10^{-2}$	
4.00 – 8.00	0.75 – 1.00	$3.75_{-0.89}^{+1.26} \times 10^{-2}$	$3.26_{-0.95}^{+0.83} \times 10^{-2}$	
4.00 – 8.00	1.00 – 1.25	$2.46_{-0.65}^{+0.56} \times 10^{-2}$	$2.14_{-0.41}^{+0.61} \times 10^{-2}$	
4.00 – 8.00	1.25 – 1.50	$1.94_{-0.44}^{+0.33} \times 10^{-2}$	$1.72_{-0.47}^{+0.37} \times 10^{-2}$	
4.00 – 8.00	1.50 – 1.75	$1.37_{-0.77}^{+0.61} \times 10^{-2}$	$1.58_{-0.37}^{+0.43} \times 10^{-2}$	

Table 2 *continued*

Table 2 (continued)

Period	Radius	Combined Detection &		No Vetting	
		(days)	(R_{\oplus})	Vetting Efficiency	Efficiency
4.00 – 8.00	1.75 – 2.00			$7.0^{+6.0}_{-4.3} \times 10^{-3}$	$5.6^{+3.1}_{-2.9} \times 10^{-3}$
4.00 – 8.00	2.00 – 2.50			$1.03^{+0.43}_{-0.18} \times 10^{-2}$	$1.10^{+0.41}_{-0.30} \times 10^{-2}$
4.00 – 8.00	2.50 – 3.00			$1.08^{+0.32}_{-0.26} \times 10^{-2}$	$1.09^{+0.38}_{-0.35} \times 10^{-2}$
4.00 – 8.00	3.00 – 4.00			$3.0^{+1.9}_{-1.2} \times 10^{-3}$	$3.3^{+1.8}_{-1.6} \times 10^{-3}$
4.00 – 8.00	4.00 – 6.00			$1.35^{+1.25}_{-0.73} \times 10^{-3}$	$1.59^{+1.09}_{-0.71} \times 10^{-3}$
4.00 – 8.00	6.00 – 8.00			$5.9^{+4.0}_{-4.5} \times 10^{-4}$	$6.8^{+4.8}_{-4.5} \times 10^{-4}$
4.00 – 8.00	8.00 – 12.00			$1.20^{+0.94}_{-0.66} \times 10^{-3}$	$1.15^{+0.86}_{-0.60} \times 10^{-3}$
4.00 – 8.00	12.00 – 16.00			$1.34^{+1.10}_{-0.41} \times 10^{-3}$	$1.78^{+0.59}_{-0.75} \times 10^{-3}$
8.00 – 16.00	0.50 – 0.75			$8.3^{+5.1}_{-4.4} \times 10^{-2}$	$6.0^{+2.0}_{-2.5} \times 10^{-2}$
8.00 – 16.00	0.75 – 1.00			$5.00^{+2.07}_{-0.87} \times 10^{-2}$	$5.1^{+1.1}_{-1.6} \times 10^{-2}$
8.00 – 16.00	1.00 – 1.25			$3.8^{+1.9}_{-1.5} \times 10^{-2}$	$3.16^{+0.62}_{-0.98} \times 10^{-2}$
8.00 – 16.00	1.25 – 1.50			$3.24^{+0.96}_{-1.11} \times 10^{-2}$	$3.10^{+0.74}_{-0.66} \times 10^{-2}$
8.00 – 16.00	1.50 – 1.75			$2.17^{+0.46}_{-0.94} \times 10^{-2}$	$2.20^{+0.60}_{-0.82} \times 10^{-2}$
8.00 – 16.00	1.75 – 2.00			$1.11^{+0.74}_{-0.70} \times 10^{-2}$	$8.8^{+5.7}_{-4.6} \times 10^{-3}$
8.00 – 16.00	2.00 – 2.50			$3.31^{+0.64}_{-0.60} \times 10^{-2}$	$3.36^{+0.89}_{-0.71} \times 10^{-2}$
8.00 – 16.00	2.50 – 3.00			$2.52^{+0.73}_{-0.60} \times 10^{-2}$	$2.64^{+0.55}_{-0.50} \times 10^{-2}$
8.00 – 16.00	3.00 – 4.00			$7.4^{+4.5}_{-3.0} \times 10^{-3}$	$8.0^{+3.4}_{-3.0} \times 10^{-3}$
8.00 – 16.00	4.00 – 6.00			$3.4^{+2.0}_{-1.8} \times 10^{-3}$	$3.5^{+1.9}_{-1.1} \times 10^{-3}$
8.00 – 16.00	6.00 – 8.00			$8.7^{+8.1}_{-5.3} \times 10^{-4}$	$1.04^{+0.94}_{-0.72} \times 10^{-3}$
8.00 – 16.00	8.00 – 12.00			$1.65^{+0.98}_{-0.92} \times 10^{-3}$	$1.49^{+1.00}_{-0.71} \times 10^{-3}$
8.00 – 16.00	12.00 – 16.00			$9.1^{+5.3}_{-4.9} \times 10^{-4}$	$1.22^{+0.69}_{-0.83} \times 10^{-3}$
16.00 – 32.00	0.50 – 0.75			$< 1.6 \times 10^{-1}$	$< 8.6 \times 10^{-2}$
16.00 – 32.00	0.75 – 1.00			$8.3^{+5.7}_{-2.3} \times 10^{-2}$	$6.3^{+3.5}_{-1.9} \times 10^{-2}$
16.00 – 32.00	1.00 – 1.25			$4.8^{+2.5}_{-2.1} \times 10^{-2}$	$3.36^{+1.97}_{-0.74} \times 10^{-2}$
16.00 – 32.00	1.25 – 1.50			$2.5^{+1.3}_{-1.3} \times 10^{-2}$	$1.97^{+0.92}_{-0.98} \times 10^{-2}$
16.00 – 32.00	1.50 – 1.75			$2.83^{+0.92}_{-1.21} \times 10^{-2}$	$2.69^{+0.62}_{-1.04} \times 10^{-2}$
16.00 – 32.00	1.75 – 2.00			$5.8^{+5.2}_{-4.0} \times 10^{-3}$	$4.3^{+4.6}_{-2.8} \times 10^{-3}$
16.00 – 32.00	2.00 – 2.50			$5.50^{+0.74}_{-0.90} \times 10^{-2}$	$5.46^{+0.74}_{-0.93} \times 10^{-2}$
16.00 – 32.00	2.50 – 3.00			$3.74^{+0.82}_{-0.78} \times 10^{-2}$	$3.72^{+1.26}_{-0.71} \times 10^{-2}$
16.00 – 32.00	3.00 – 4.00			$2.21^{+0.70}_{-0.48} \times 10^{-2}$	$2.33^{+0.54}_{-0.65} \times 10^{-2}$
16.00 – 32.00	4.00 – 6.00			$3.3^{+1.8}_{-2.0} \times 10^{-3}$	$3.8^{+2.0}_{-2.1} \times 10^{-3}$
16.00 – 32.00	6.00 – 8.00			$2.4^{+1.9}_{-1.4} \times 10^{-3}$	$2.1^{+2.0}_{-1.3} \times 10^{-3}$
16.00 – 32.00	8.00 – 12.00			$2.1^{+1.6}_{-1.3} \times 10^{-3}$	$2.7^{+1.1}_{-1.5} \times 10^{-3}$
16.00 – 32.00	12.00 – 16.00			$2.3^{+1.6}_{-1.2} \times 10^{-3}$	$2.2^{+2.5}_{-1.0} \times 10^{-3}$
32.00 – 64.00	0.50 – 0.75			$< 2.1 \times 10^{-1}$	$< 1.7 \times 10^{-1}$
32.00 – 64.00	0.75 – 1.00			$5.2^{+2.7}_{-3.3} \times 10^{-2}$	$3.2^{+4.0}_{-1.5} \times 10^{-2}$
32.00 – 64.00	1.00 – 1.25			$6.0^{+4.0}_{-2.4} \times 10^{-2}$	$4.4^{+3.0}_{-1.7} \times 10^{-2}$
32.00 – 64.00	1.25 – 1.50			$1.07^{+1.02}_{-0.61} \times 10^{-2}$	$9.0^{+9.7}_{-7.1} \times 10^{-3}$
32.00 – 64.00	1.50 – 1.75			$2.07^{+0.89}_{-1.06} \times 10^{-2}$	$1.82^{+1.37}_{-0.75} \times 10^{-2}$
32.00 – 64.00	1.75 – 2.00			$1.27^{+0.74}_{-0.77} \times 10^{-2}$	$9.7^{+15.1}_{-7.4} \times 10^{-3}$

Table 2 continued

Table 2 (*continued*)

Period	Radius	Combined Detection &	No Vetting
		Vetting Efficiency	
32.00 – 64.00	2.00 – 2.50	$5.4^{+1.5}_{-1.2} \times 10^{-2}$	$5.2^{+1.0}_{-1.4} \times 10^{-2}$
32.00 – 64.00	2.50 – 3.00	$6.2^{+1.2}_{-1.0} \times 10^{-2}$	$6.4^{+1.1}_{-1.4} \times 10^{-2}$
32.00 – 64.00	3.00 – 4.00	$2.25^{+0.85}_{-0.69} \times 10^{-2}$	$2.04^{+0.77}_{-0.66} \times 10^{-2}$
32.00 – 64.00	4.00 – 6.00	$3.7^{+2.6}_{-1.9} \times 10^{-3}$	$3.4^{+2.9}_{-1.8} \times 10^{-3}$
32.00 – 64.00	6.00 – 8.00	$6.1^{+1.9}_{-2.7} \times 10^{-3}$	$5.0^{+2.6}_{-2.3} \times 10^{-3}$
32.00 – 64.00	8.00 – 12.00	$3.2^{+3.9}_{-1.7} \times 10^{-3}$	$2.7^{+1.9}_{-1.4} \times 10^{-3}$
32.00 – 64.00	12.00 – 16.00	$5.0^{+3.0}_{-2.6} \times 10^{-3}$	$5.2^{+2.7}_{-2.5} \times 10^{-3}$
64.00 – 128.00	0.50 – 0.75	$< 1.0 \times 10^0$	$< 9.3 \times 10^{-1}$
64.00 – 128.00	0.75 – 1.00	$< 1.3 \times 10^{-1}$	$< 1.5 \times 10^{-1}$
64.00 – 128.00	1.00 – 1.25	$1.12^{+0.50}_{-0.58} \times 10^{-1}$	$8.9^{+6.3}_{-4.7} \times 10^{-2}$
64.00 – 128.00	1.25 – 1.50	$2.2^{+6.6}_{-1.7} \times 10^{-2}$	$1.31^{+0.75}_{-0.98} \times 10^{-2}$
64.00 – 128.00	1.50 – 1.75	$2.1^{+1.8}_{-1.5} \times 10^{-2}$	$2.0^{+2.0}_{-1.2} \times 10^{-2}$
64.00 – 128.00	1.75 – 2.00	$1.29^{+0.03}_{-0.52} \times 10^{-2}$	$1.88^{+1.68}_{-0.99} \times 10^{-2}$
64.00 – 128.00	2.00 – 2.50	$6.5^{+2.1}_{-2.0} \times 10^{-2}$	$5.5^{+1.5}_{-1.4} \times 10^{-2}$
64.00 – 128.00	2.50 – 3.00	$3.7^{+1.4}_{-1.3} \times 10^{-2}$	$3.7^{+1.4}_{-1.2} \times 10^{-2}$
64.00 – 128.00	3.00 – 4.00	$3.6^{+1.1}_{-1.1} \times 10^{-2}$	$3.36^{+1.14}_{-1.00} \times 10^{-2}$
64.00 – 128.00	4.00 – 6.00	$1.51^{+0.76}_{-0.70} \times 10^{-2}$	$1.47^{+0.75}_{-0.61} \times 10^{-2}$
64.00 – 128.00	6.00 – 8.00	$5.1^{+3.9}_{-3.2} \times 10^{-3}$	$3.7^{+3.6}_{-2.2} \times 10^{-3}$
64.00 – 128.00	8.00 – 12.00	$9.3^{+5.6}_{-3.9} \times 10^{-3}$	$8.4^{+3.6}_{-3.3} \times 10^{-3}$
64.00 – 128.00	12.00 – 16.00	$4.5^{+3.2}_{-2.7} \times 10^{-3}$	$3.5^{+3.4}_{-1.8} \times 10^{-3}$
128.00 – 256.00	0.50 – 0.75	$< 9.5 \times 10^{-1}$	$< 8.3 \times 10^{-1}$
128.00 – 256.00	0.75 – 1.00	$< 5.8 \times 10^{-1}$	$< 5.0 \times 10^{-1}$
128.00 – 256.00	1.00 – 1.25	$< 1.8 \times 10^{-1}$	$< 1.7 \times 10^{-1}$
128.00 – 256.00	1.25 – 1.50	$< 9.1 \times 10^{-2}$	$< 4.8 \times 10^{-2}$
128.00 – 256.00	1.50 – 1.75	$3.2^{+2.6}_{-2.2} \times 10^{-2}$	$3.3^{+2.5}_{-1.8} \times 10^{-2}$
128.00 – 256.00	1.75 – 2.00	$2.2^{+2.6}_{-1.4} \times 10^{-2}$	$2.3^{+3.0}_{-1.1} \times 10^{-2}$
128.00 – 256.00	2.00 – 2.50	$5.6^{+3.1}_{-2.4} \times 10^{-2}$	$6.0^{+2.4}_{-2.4} \times 10^{-2}$
128.00 – 256.00	2.50 – 3.00	$7.8^{+2.7}_{-2.5} \times 10^{-2}$	$7.1^{+1.8}_{-2.3} \times 10^{-2}$
128.00 – 256.00	3.00 – 4.00	$2.9^{+1.7}_{-1.3} \times 10^{-2}$	$2.98^{+0.83}_{-1.27} \times 10^{-2}$
128.00 – 256.00	4.00 – 6.00	$9.2^{+7.5}_{-4.5} \times 10^{-3}$	$8.9^{+6.8}_{-3.2} \times 10^{-3}$
128.00 – 256.00	6.00 – 8.00	$1.15^{+1.14}_{-0.67} \times 10^{-2}$	$8.8^{+5.0}_{-3.7} \times 10^{-3}$
128.00 – 256.00	8.00 – 12.00	$1.81^{+1.05}_{-0.91} \times 10^{-2}$	$1.88^{+0.81}_{-0.71} \times 10^{-2}$
128.00 – 256.00	12.00 – 16.00	$< 7.8 \times 10^{-3}$	$< 8.2 \times 10^{-3}$
256.00 – 500.00	0.50 – 0.75	$< 8.0 \times 10^{-1}$	$< 7.7 \times 10^{-1}$
256.00 – 500.00	0.75 – 1.00	$< 6.1 \times 10^{-1}$	$< 5.0 \times 10^{-1}$
256.00 – 500.00	1.00 – 1.25	$< 3.6 \times 10^{-1}$	$< 3.1 \times 10^{-1}$
256.00 – 500.00	1.25 – 1.50	$< 2.2 \times 10^{-1}$	$< 1.8 \times 10^{-1}$
256.00 – 500.00	1.50 – 1.75	$1.8^{+1.3}_{-1.2} \times 10^{-1}$	$1.15^{+1.35}_{-0.65} \times 10^{-1}$
256.00 – 500.00	1.75 – 2.00	$1.69^{+0.98}_{-0.89} \times 10^{-1}$	$1.08^{+0.88}_{-0.58} \times 10^{-1}$
256.00 – 500.00	2.00 – 2.50	$5.4^{+6.2}_{-3.9} \times 10^{-2}$	$4.4^{+1.8}_{-2.3} \times 10^{-2}$

Table 2 *continued*

Table 2 (continued)

Period	Radius	Combined Detection & Vetting Efficiency	No Vetting
(days)	(R_{\oplus})	Vetting Efficiency	Efficiency
256.00–500.00	2.50– 3.00	$7.5^{+4.4}_{-3.3} \times 10^{-2}$	$5.8^{+3.1}_{-1.6} \times 10^{-2}$
256.00–500.00	3.00– 4.00	$5.1^{+3.2}_{-2.5} \times 10^{-2}$	$3.4^{+3.5}_{-1.1} \times 10^{-2}$
256.00–500.00	4.00– 6.00	$2.6^{+1.6}_{-1.7} \times 10^{-2}$	$3.1^{+2.2}_{-1.4} \times 10^{-2}$
256.00–500.00	6.00– 8.00	$< 2.0 \times 10^{-2}$	$< 1.1 \times 10^{-2}$
256.00–500.00	8.00–12.00	$2.00^{+0.85}_{-0.92} \times 10^{-2}$	$1.72^{+1.22}_{-0.78} \times 10^{-2}$
256.00–500.00	12.00–16.00	$< 2.0 \times 10^{-2}$	$< 1.8 \times 10^{-2}$

NOTE—Estimated occurrence rates for DR25 KOI catalog planet candidates associated with FGK stars using two different vetting efficiency schemes.

4. DISCUSSION

Using Kepler DR25, Gaia DR2, SysSim and ABC model, we provide accurate estimates of the exoplanet occurrence rate around FGK main sequence stars as a function of planet size and orbital period. Our results span a wide range of orbital periods and planet radii, including the η_{\oplus} regime, without the need to extrapolate. Our Bayesian approach provides direct and meaningful constraints on the η_{\oplus} regime, despite the limited number of such planet candidates (see §4.2). We find planet occurrence rates somewhat lower than some previous studies (e.g., Figure 17 of Burke et al. 2015). This may have significant implications for scientists planning future planet surveys or characterization missions.

We performed extensive tests of our model and examined the relative importance of various upgrades to the model. One of the most significant factors resulting in differences with the Q1–Q16 rates presented in Hsu et al. (2018) is the usage of Gaia DR2 stellar parameters. In addition to improving the accuracy of planet radii, the Gaia data enabled the selection of a clean sample of FGK main sequence target stars for occurrence rate studies. The number of small planets at long orbital periods was significantly reduced after focusing on a clean FGK target star sample and incorporating improved stellar radii. This is one factor that contributes to our inferred occurrence rates being lower than many previous studies.

We find that it is important to account for the vetting efficiency when characterizing the occurrence rate of small planets or planets with orbital periods greater than a month (see §4.1). Further, we caution that one previously proposed model for the vetting efficiency can result in significantly overestimating the rate of planets in the η_{\oplus} regime by $\simeq 20–40\%$ relative to a model directly fit to result of transit injection studies. We provide an improved model for the combined detection efficiency (i.e., including both being

identified by the Kepler planet search pipeline and labeled as a planet candidate by the robovetter) in Eqn. 3.

We conclude with a discussion of the areas for further improvement in future occurrence rate studies (§4.3) and implications for mission planning (§4.3.1).

4.1. Implications of Vetting Efficiency

Previous studies of planet occurrence rates have assumed that all true planets detected by Kepler’s Transiting Planet Search module are labeled as planet candidates in the Kepler planet catalog. With Kepler’s DR25 data release, vetting of threshold crossing events was performed by an automated process, the “robovetter”. This opened the door to explicitly modeling the vetting efficiency, i.e. the probability with which the Kepler robovetter identifies a true exoplanet as a planet candidate.

In order to explore the importance of vetting efficiency, we calculated the occurrence rate using three different models:

- Using the detection efficiency model in Eqn. 1 and setting the vetting efficiency to unity. This is analogous to previous exoplanet occurrence rate studies.
- Using the detection efficiency model in Eqn. 1 and adopting the vetting efficiency in Eqn. 2, a function of orbital period and planet radius proposed by Mulders et al. (2018).
- Using a single model for the combined detection and vetting efficiency in Eqn. 3.

The occurrence rates produced by these three different models are compared for two bins in different detection regimes in Fig. 4. When comparing results using a vetting efficiency of unity to results using the Mulders vetting efficiency model, we find that the Mulders model can result in large increase in the inferred planet occurrence rate, particularly for small, long-period planets (bottom panel). In several cases, the difference in inferred rates is larger than the statistical uncertainties. As the occurrence rate of such planets is of particular

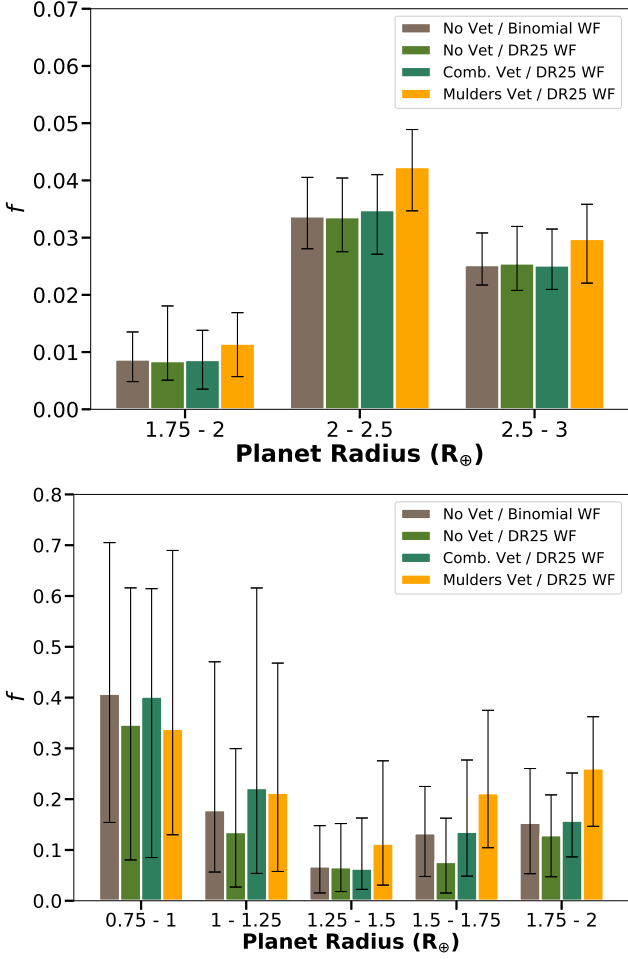


Figure 4. Occurrence rate estimates over several radii bins over the range (Top) $P = 8 - 16$ d and (Bottom) $P = 237 - 500$ d with different vetting efficiencies and window functions using a uniform prior with individual bin parameterization. The upper panel is representative of the majority of the grid in planet size and orbital period, where the planet occurrence rates are well-constrained and the choice of window function and vetting efficiency model has a small impact on the inferred planet occurrence rate. However, both the window function and model for vetting efficiency are important for planets with longer orbital periods, as illustrated in the bottom panel. The DR25 catalog does not include any planet candidates (associated with our cleaned sample of Kepler targets) in the bins with $P = 237 - 500$ d and $R_p = \{0.75 - 1, 1 - 1.25, 1.25 - 1.5\} R_\oplus$. Therefore, the posterior distribution in these bins is broad and sensitive to the choice of prior. Nevertheless, the lack of detections provides robust upper limits on the planet occurrence rates in these bins. Our baseline results are based on using the DR25 window function and the combined detection and vetting efficiency model, as it was directly fit to pixel-level transit injection simulations.

interest, this motivated us to develop an improved model for the vetting efficiency. We make use of the pixel-level transit injections that were processed by both the Kepler planet search pipeline and the robovetter to empirically fit a model

for the probability of a true transiting planet being both detected by the pipeline and labeled as a planet candidate.

Our results demonstrate the importance of both accounting for the vetting efficiency and of using an accurate vetting efficiency model. When comparing the results with our model for the combined detection and vetting efficiency, we find significant changes in the inferred planet occurrence rates relative to previous calculations that neglected vetting efficiency, only for bins with $P > 32$ d or $R_p < 2R_\oplus$. For the remainder of the bins, the difference in the median of the ABC-posteriors is typically considerably less than the width of the ABC-posterior.

When comparing the results using our combined detection and vetting efficiency to results using the Mulders model, we find that the Mulders model typically overestimates occurrence rates of sub-Neptune-size planets by $\sim 20\%$ to 40% relative to our model for the particular size and period ranges shown in this comparison. We interpret this as an artifact of the functional form adopted in the Mulders model which is a function of orbital period and planet size, without accounting for the transit SNR or number of transits observed.

4.2. Occurrence Rates of Planets near the Habitable Zone

Given the widespread interest in the occurrence rate of small planets in or near the habitable zone (η_\oplus), we performed additional calculations for the occurrence rate of planets with radii $\{0.75 - 1, 1 - 1.25, 1.25 - 1.5, 1.5 - 1.75, 1.75 - 2\} R_\oplus$ and orbital periods 237-500 days using different choices of window functions and vetting efficiencies.

4.2.1. Importance of Individual Model Improvements

Our results using an independent uniform prior for each bin's occurrence rate can be seen in Fig. 4 (lower panel) where we present occurrence rate estimates assuming: 1) no loss of planets due to the vetting process and the simple binomial window function (comparable to the methodology of Hsu et al. (2018)), 2) no loss of planets due to the vetting process and DR25 target-by-target window functions, 3) combined detection and vetting efficiency and DR25 target-by-target window functions, and 4) Mulders et al. (2018) vetting efficiency and DR25 target-by-target window functions.

The inclusion of a target-by-target set of window functions can result in diminishing the inferred occurrence rates in the η_\oplus regime due to better accounting for detection probability when there are few transits. Even for planets with periods of 237-500 d and radii of $0.75 - 1.75 R_\oplus$, we show that this effect on occurrence rates is relatively modest.

Accounting for the vetting efficiency can significantly affect the inferred occurrence rate compared to previous estimates that have assumed all planets pass the vetting process. The occurrence rates based on the combined detection and vetting efficiency model generally increases relative to

assuming perfect vetting. However, we find that the application of the [Mulders et al. \(2018\)](#) vetting efficiency model would lead to overestimating the occurrence rate relative to our model for a combined detection and vetting efficiency for planets with radii $1.25\text{--}2 R_{\oplus}$ and periods of $237\text{--}500d$. This demonstrates the importance of developing an accurate model for the vetting process.

For orbital periods beyond 128 days, Kepler observations place interesting upper limits on the occurrence rate of Earth-size planets, even if there are no detections in a given period-radius bin. Table 2 and Figure 2 provide upper limits based on adopting independent uniform priors for each bin's occurrence rate. While appealing in its simplicity, adopting independent uniform priors for each bin is equivalent to assuming a total rate of planets in that period range that is strongly peaked at large planet occurrence rates. While the choice of prior did not have a significant effect for most of the bins in our period-radius grid, it does affect the rates derived in the η_{\oplus} regime. Given the relatively weak observational constraints, the use of a peaked prior on the total rate of small planets in the habitable zone seems unwise.

Therefore, for the results presented in §4.2.2, we performed additional simulations specifically focusing on this regime using a Dirichlet prior over radius bins with boundaries subset $R_p = \{0.5, 0.75, 1, 1.25, 1.5, 1.75, 2, 2.5\}$. This allows us to compute the posterior distribution for the rate of small, long-period planets, while assuming a uniform prior on the rate of planets of all sizes between 0.5 and $2.5 R_{\oplus}$. The rate of planets in each bin larger than $2.5 R_{\oplus}$ is well constrained and the sum is less than $\simeq 40\%$. One could attempt to use the rate of larger planets to motivate a narrower prior on the rate of planets between 0.5 and $2.5 R_{\oplus}$. However, we do not reduce the upper limit for the total rate in $P = 237\text{--}500d$ and $R_p = 0.5\text{--}2.5 R_{\oplus}$ planets, as any corrections would be modest and the reliability of the larger planet candidates may not be well known.

4.2.2. η_{\oplus} Rate Estimates

Our ABC posterior distributions for η_{\oplus} (or Γ_{\oplus}) summarize the current state of our knowledge about the rate of small planets in the habitable zone of FGK stars (see panels a, c, e, g, i and k of Figure 5). We summarize our results by reporting upper limits (84.13th percentile) and median (50th percentile) occurrence rate of small planets over the period range $P = 237\text{--}500d$ using our combined detection and vetting efficiency and two choices of prior. Note that the our recommended rates in this regime are based on the Dirichlet prior for relative rates, and so these rates differ from the rates reported in Table 2 and Figure 2 based on independent uniform priors for each bin. Comparing the results with the two priors can be useful as a test to establish how sensitive these occurrence rates are to the choice of prior. Summing over the

three interior bins, the $\{5, 15.87, 50, 84.13, 95\}$ th percentiles for the summed occurrence rate assuming the Dirichlet prior over the range $P = 237\text{--}500d$, $R_p = 1\text{--}1.75 R_{\oplus}$ are $f_{R,P} = \{0.09, 0.14, 0.24, 0.35, 0.46\}$. The corresponding percentiles for the differential rates are $\Gamma_{\oplus} \equiv (d^2 f)/[d(\ln P) d(\ln R_p)] = \{0.22, 0.34, 0.57, 0.84, 1.1\}$ for the same range. We consider the above rates to represent the current best estimates.

For the sake of examining the sensitivity of the results to the choice of prior, we performed a similar analysis, adopting an independent uniform prior for each radius bin. The results can be seen in panels b, d, f, h, j and l of Figure 5. Using this prior, the $\{5, 15.87, 50, 84.13, 95\}$ th percentiles for the summed occurrence rate over the range $P = 237\text{--}500d$, $R_p = 1\text{--}1.75 R_{\oplus}$ are $f_{R,P} = \{0.16, 0.22, 0.36, 0.56, 0.70\}$ while the differential rates are $\Gamma_{\oplus} = \{0.38, 0.53, 0.87, 1.4, 1.7\}$. While we expect use of independent uniform priors to result in an overestimate of summed occurrence rates, we include these values to quantify the sensitivity of these results to the choice of prior. While these two priors are quite different (e.g., compare dotted lines for panels k & l), the ABC posteriors are qualitatively similar for large rates (where data provide strong constraints), but differ significantly for small rates (where the posterior shape is primarily based on information coming from the prior).

The median of our posterior for the occurrence rate of small planets in or near the habitable zone of sun-like stars (see Figure 5, panel k) is similar to estimates based on extrapolation from recent studies and well with in the range of possibilities suggested by sensitivity analyses (e.g., Figure 17 of [Burke et al. 2015](#)). Our upper limits are significantly tighter than previous upper limits, due to a combination of effects including the use of Kepler's final DR25 planet candidate catalog, updated stellar properties from Gaia, and use of DR25 data products such as the target-specific window functions. While our upper limits should be robust, the lower limits are sensitive to the choice of prior and the unknown reliability of planet candidates in this regime (see §4.3 & [Thompson et al. 2018](#)).

4.2.3. Extrapolations to Longer Periods

While some previous studies have offered estimates of η_{\oplus} for FGK stars ([Petigura et al. 2013](#); [Foreman-Mackey et al. 2014](#); [Burke et al. 2015](#); [Mulders et al. 2018](#), e.g.,), we caution that such estimates involved extrapolating a model that is constrained based on planets with larger sizes and/or shorter orbital periods. While it's possible that the occurrence rate of planets as a function of planet size and period varies sufficiently slowly to render such extrapolations accurate, there are both observational and theoretical reasons to be cautious about such extrapolations. Theoretically, the origin and evolution of planets with significant gas envelopes could quite different than that of rocky planets. Indeed, studies have sug-

Table 3. HZ Occurrence Rate Estimates

Radius (R_{\oplus})	Prior	
	Dirichlet	Uniform
0.75 – 1.00	< 0.22	< 0.7
1.00 – 1.25	< 0.087	< 0.31
1.25 – 1.50	< 0.075	< 0.14
1.50 – 1.75	$0.15^{+0.10}_{-0.09}$	$0.12^{+0.09}_{-0.07}$
1.75 – 2.00	$0.082^{+0.076}_{-0.069}$	$0.14^{+0.08}_{-0.07}$
1.00 – 1.75	$0.24^{+0.11}_{-0.10}$	$0.36^{+0.20}_{-0.14}$

NOTE—Occurrence rate estimates over the HZ region for $P = 237 - 500$ d and several radii bins with two prior choices. Upper limits correspond to the 84.13th percentile.

gested a local minimum in the occurrence rates as a function of planet size, perhaps due to photoevaporation or core-powered mass-loss (Owen & Wu 2017; Gupta & Schlichting 2018). Such a feature is not captured by parametric models which assume planet occurrence rates to be proportional to a power-law (or broken power-law) in planet radius. Additionally, there may be qualitative changes in the occurrence rate and properties of planets as orbital periods approach that of the ice line. From an observational perspective, radial velocity surveys find a substantial rise in the frequency of more massive planets starting at orbital periods close to one year. Similarly, we find the occurrence rate of larger planets increases substantially as orbital periods increase beyond ~ 128 d. Therefore, we recommend that scientists and mission planners be cautious in adopting estimates of η_{\oplus} that are primarily the result of extrapolating a parametric model into the η_{\oplus} regime.

Instead, we recommend making use of the ABC-posterior distribution for η_{\oplus} (or Γ_{\oplus}) which encapsulates the current direct observational constraints of the occurrence rate of small planets in the habitable zone of FGK stars. This represents a direct measurement based on Kepler data for the relevant planet sizes and orbital periods and not an extrapolation. Our constraints on η_{\oplus} are only possible thanks to the Kepler project providing DR 25 data products for both actual Kepler data and simulated data with injected transits.

For purposes of planning missions to directly image potentially Earth-like planets, mission concepts are computing expected mission yields based on the ranges $P = 338 - 788$ d and $R_p = 0.8 - 1.4R_{\oplus}$ for a solar twin. Unfortunately, Kepler’s mission duration and sensitivity do not place meaningful constraints on small planets at such long orbital periods. If one were to extrapolate our results using the Dirichlet prior, assuming the differential occurrence rate derived

over the interval $P = 237 - 500$ d and $R_p = 0.75 - 1.5$, then one obtains an upper limit (95th percentile) of 0.43 planets per sun-like star with $P = 338 - 788$ d and $R_p = 0.8 - 1.4R_{\oplus}$. As described above, we recommend considerable caution when adopting occurrence rates that are based on an extrapolation from shorter orbital periods. In this case, the inclusion of long-period planets with sizes less than $1 R_{\oplus}$, results in the results of such an extrapolation being sensitive to the choice of prior. For example, adopting independent uniform priors for the rates of each radius bin results in the 95th percentile of the posterior increasing to 1.2 planets per sun-like star with $P = 338 - 788$ d and $R_p = 0.8 - 1.4R_{\oplus}$.

4.3. Future Prospects for Occurrence Rate Studies

The model used in this study could be improved further to account for additional effects. We summarize the assumptions of our current model and our rationale for postponing consideration of these effects.

Detection Model: We model the probability that a planet is detected as a function of the expected effective SNR and the number of transits observed. In principle, the detection model could be further improved to incorporate additional information (e.g., transit duration, stellar properties, sky group).

Uncertainty in Contamination: This study models the effects of contamination due to known stars, but does not account for the uncertainty in the contamination. If only a fraction of the flux observed for a given Kepler target comes from the planet-hosting star, then the transit depth is diluted by the contaminating flux. While this has been considered in detail for individual systems (Hirsch et al. 2017; Teske et al. 2018), it is unclear how much contamination affects planet occurrence rate studies. In this study, we account for the dilution of transit depths due to contamination from known stars when

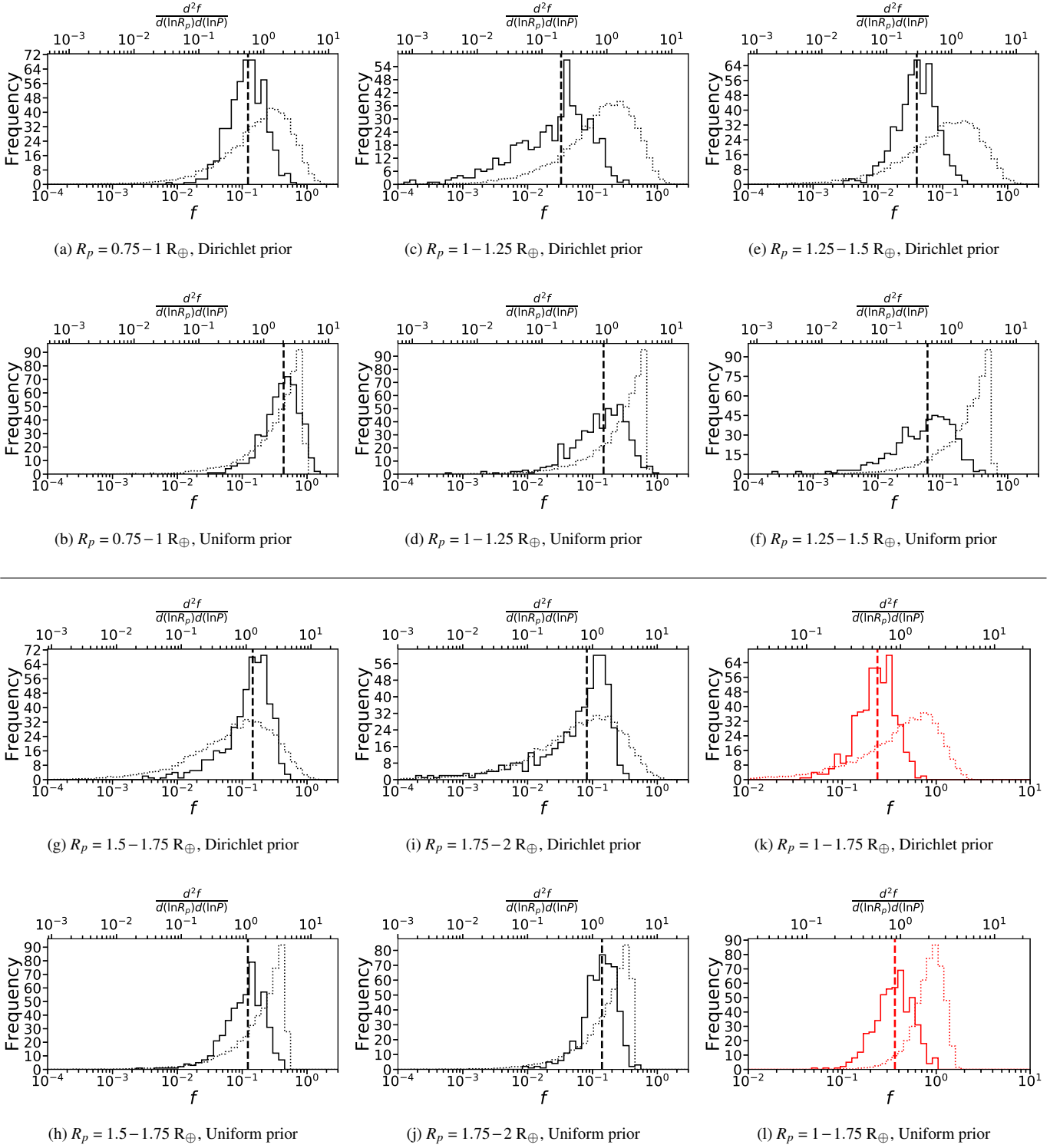


Figure 5. ABC posterior samples for the planet occurrence for planets with orbital periods of $P = 237 - 500$ d around FGK stars using two prior choices. The panels show results for several radius bins in the η_{\oplus} regime using the combined detection and vetting efficiency with two choices of prior. For comparison, a sample from the prior distribution is shown by the dotted line. The median (i.e. 50th percentile) is indicated by the vertical dashed line. For all size ranges shown, the inferred upper limits (e.g. 84.13th or 95th percentiles) are significantly less than the same percentile for the prior, even for radius ranges that do not include any detected planet candidate. Panels a - f show bins where Kepler detected no planets (for targets included in our cleaned sample) while panels g - j show bins with Kepler planet candidates. Panels k & l (bottom right) show the integrated rate over $1 - 1.75 R_{\oplus}$ (assuming the occurrence rate is piecewise constant over each of $1 - 1.25$, $1.25 - 1.5$, and $1.5 - 1.75 R_{\oplus}$). The posterior mode is near 0.3 such planets per star. More importantly, Kepler data provides a 95th percentile empirical upper limit of 0.46 (Dirichlet prior) and 0.70 (Uniform prior) on the rate of such planets.

computing the transit depth and SNR. We adopt the contamination provided for each target in the Kepler Input Catalog (KIC). Of course, there may be additional dilution from unknown sources, particularly bound multiple star systems. We mitigate the effects of unrecognized contamination from multiple star systems by focusing our analysis on a subset of the Kepler target stars which excludes targets with either astrometric data suggestive of binary companion or that appear to reside significantly above the main sequence. While binary stars with more disparate luminosities will survive our target selection process, they have limited effect on the planet occurrence rate. If a planet transits a star significantly fainter than the primary star, then the detection probability is significantly reduced by contamination from the primary. Therefore, such planets will rarely be detected for targets in our cleaned target list. If a planet transits the primary star in a system with a significantly fainter secondary star, then the effect of dilution is modest. Therefore, we expect that the size of the effect of unrecognized dilution will have a modest effect on the occurrence rates inferred using our cleaned target list.

Multiple Transiting Planets & TCEs: For targets with multiple transiting planets, the Kepler pipeline searched for planet candidates in an iterative fashion. After each “threshold crossing event” (TCE) was identified, the pipeline masked out a portion of the lightcurve during and immediately surrounding each putative transit before searching for additional planet candidates. The pipeline selected larger MES candidates first so that the presence of a larger and/or shorter-period planet causes the effective duty cycle to be reduced when searching for lower MES signals around the same star. Further complicating matters, the pipeline identified many TCEs that were later discarded as not being strong planet candidates. Nevertheless, all TCEs result in less data being available for detecting additional planets transiting that target (Zink et al. 2019). Fully accounting for these effects would be extremely complicated due to the complexity of the pipeline, and the available data products. Further, the measurement of planet occurrence rates would no longer decouple from the characterization of planetary system architectures. An initial investigation of this effect, suggested that the detectability of planets may decrease by $\simeq 5.5\%$ (15.9%) for planets with orbital periods less (greater) than 200 days, if the system contains another transiting planet which the pipeline would detect first (Zink et al. 2019). The DR25 pipeline run resulted in 34,032 TCEs, far greater than the then $\simeq 8,000$ KOIs (Twicken et al. 2016). Since our combined detection and vetting efficiency is based on fitting to the results of pixel-level transit injections into light curves that already include these TCEs, our detection efficiency already accounts for this, but in an average sense, rather than using knowledge of specific TCEs for each star.

The decrease in detectability due to additional planets only affects a small fraction of stars, since the ratio of planet candidates to target stars is $\simeq 0.03$ in our sample. If all planetary systems were strictly coplanar, then short-period planets would transit whenever the long-period planet transited. However, for orbital periods of 237-500 days, even very modest mutual inclinations ($\simeq 1^\circ$) cause the conditional transit probability to decrease substantially. Therefore, the impact of this effect on the overall planet occurrence rate will be diluted by at least half, even if this effect is significant for analyzing the relative abundance of systems with single and multiple transiting planets. In summary, we estimate that any increase in the occurrence rate of long-period planets due to interactions of the Kepler pipeline and multiple planet systems is likely to be less than $\simeq 8\%$

Pipeline Timeouts: The actual Kepler DR25 transit search did not search every target for transit signals as small as the typical 7.1σ threshold. The DR25 stellar catalog reports the “MES threshold” and “timeout” indicators for when the search for transits was halted prematurely. The DR25 stellar catalog data indicate that only 94% of targets were searched to MES of 7.1 (the standard criterion for triggering a TCE) across all durations. When applying this only to stars in our clean FGK catalog, 96% of targets were searched to full depth. However, of the 4% that were not searched to MES of 7.1, the MES threshold was still below 8 in 80% of the cases. In practice, the detection and vetting probability is so low for such cases that our assumption that the pipeline would have found detections between MES of 8 and 7.1 around these 3.2% of stars would not affect our results significantly. The remaining 0.8% of stars with somewhat higher MES thresholds are also not a significant source of systematic error.

Reliability: Our analysis assumes that all planet candidates (identified by DR25 pipeline and associated with target stars in our cleaned sample) were correctly identified as planet candidates, rather than being some sort of false positive (e.g., diluted eclipsing binary) or false alarm (e.g., astrophysical noise). Therefore, technically, the occurrence rates we infer should be regarded as the combined occurrence rate of true planets and any astrophysical false positives or instrumental false alarms that masquerade as planets within the given range of planet sizes and orbital periods. Fortunately, the overall reliability of the Kepler planet candidate sample is quite high (Thompson et al. 2018). Nevertheless, validating any individual planet candidate at high reliability is difficult (Burke et al. 2019). For bins with a small number of detected planets (e.g., small, long-period planets, but also planets with very short-periods and very large planets), a few planet candidates being a false positive or false alarm could cause our inferred rate to be larger than the true planet rate. While this could be a large fractional error, it would not contribute significantly to the total number of planets integrated

over a broad range of orbital periods and planet sizes. Reliability concerns are particularly acute at long orbital periods (e.g., our 256–500d bin), as shown in Thompson et al. (2018). Complicated interactions of detector noise and the spacecraft orbital period likely contribute to some of the planet candidates at long orbital periods. We have attempted to mitigate reliability concerns by analyzing a cleaned set of target stars. Nevertheless, we regard the apparent increase in the occurrence rate of $R=1.5-6 R_{\oplus}$ planets beyond 256d as highly suggestive, but worthy of a more detailed investigation that includes a detailed treatment of the reliability of long-period planet candidates. We note that reliability concerns will only lead to revisions downward in the inferred rate. Therefore, our upper limits on the occurrence rates of small planets are robust to reliability concerns.

For periods of 128–256d and 256–500d, upper limits for the sum of occurrence rate over all radii exceeds one planet per star. Previous studies have shown that the fraction of stars with planets is significantly less than the average number of planets per star, based largely on the observed distribution of targets with multiple transiting planets. If the reliability of these long-period planet candidates is shown to be high, then future studies should also investigate the extent to which long-term orbital stability helps to inform the upper limit on the occurrence rate of long-period planets. A high occurrence rate of large-radii planets could dynamically restrict the occurrence rate of smaller radius planets.

4.3.1. Recommendations

In conclusion, we recommend that mission concepts aiming to characterize potentially rocky planets in or near the habitable zone of sun-like stars prepare compelling science programs that would be robust to the true rate of $1-1.75 R_{\oplus}$ planets with orbital periods in 237–500 days, $f_{R,P} \simeq 0.05-0.51$ or a differential rate of $(d^2 f)/[d(\ln P) d(\ln R_p)] \simeq 0.11-1.2$. This is based on the 90% credible interval derived from our calculations, but also allows for the possibility of the reliability of such planets being as low as $\simeq 50\%$ or for

the rate to increase by up to $\simeq 10\%$ due to issues discussed above.

We thank the entire Kepler team for the many years of work that has proven so successful and was critical to this study. D.C.H, E.B.F., D.R., and K.A. acknowledge support from NASA Origins of Solar Systems grant # NNX14AI76G and Exoplanet Research Program grant # NNX15AE21. E.B.F acknowledges support from NASA Kepler Participating Scientist Program Cycle II grant # NNX14AN76G. D.C.H, E.B.F. acknowledge support from the Penn State Eberly College of Science and Department of Astronomy & Astrophysics, the Center for Exoplanets and Habitable Worlds and the Center for Astrostatistics. The citations in this paper have made use of NASA’s Astrophysics Data System Bibliographic Services. This research has made use of the NASA Exoplanet Archive, which is operated by the California Institute of Technology, under contract with the National Aeronautics and Space Administration under the Exoplanet Exploration Program. This work made use of the *gaia-kepler.fun* crossmatch database created by Megan Bedell. We acknowledge the Institute for CyberScience (<http://ics.psu.edu/>) at The Pennsylvania State University, including the CyberLAMP cluster supported by NSF grant MRI-1626251, for providing advanced computing resources and services that have contributed to the research results reported in this paper. This material was based upon work partially supported by the National Science Foundation under Grant DMS-1127914 to the Statistical and Applied Mathematical Sciences Institute (SAMSI). Any opinions, findings, and conclusions or recommendations expressed in this material are those of the author(s) and do not necessarily reflect the views of the National Science Foundation. This study benefited from the 2013 SAMSI workshop on Modern Statistical and Computational Methods for Analysis of Kepler Data, the 2016/2017 Program on Statistical, Mathematical and Computational Methods for Astronomy, and their associated working groups.

REFERENCES

- Andrae, R., Fouesneau, M., Creevey, O., et al. 2018, *A&A*, 616, A8, doi: [10.1051/0004-6361/201732516](https://doi.org/10.1051/0004-6361/201732516)
- Beaumont, M. A., Cornuet, J.-M., Marin, J.-M., & Robert, C. P. 2008, ArXiv e-prints. <https://arxiv.org/abs/0805.2256>
- Berger, T. A., Huber, D., Gaidos, E., & van Saders, J. L. 2018, *ApJ*, 866, 99, doi: [10.3847/1538-4357/aada83](https://doi.org/10.3847/1538-4357/aada83)
- Braknsiek, J., & Ragozzine, D. 2016, *ApJ*, 821, 47, doi: [10.3847/0004-637X/821/1/47](https://doi.org/10.3847/0004-637X/821/1/47)
- Burke, C. J., & Catanzarite, J. 2017a, Planet Detection Metrics: Window and One-Sigma Depth Functions for Data Release 25, Tech. rep.
- . 2017b, Planet Detection Metrics: Per-Target Flux-Level Transit Injection Tests of TPS for Data Release 25, Tech. rep.
- . 2017c, Planet Detection Metrics: Per-Target Detection Contours for Data Release 25, Tech. rep.
- Burke, C. J., Mullally, F., Thompson, S. E., Coughlin, J. L., & Rowe, J. F. 2019, arXiv e-prints, arXiv:1901.00506. <https://arxiv.org/abs/1901.00506>

- Burke, C. J., Christiansen, J. L., Mullally, F., et al. 2015, *ApJ*, 809, 8, doi: [10.1088/0004-637X/809/1/8](https://doi.org/10.1088/0004-637X/809/1/8)
- Christiansen, J. L. 2017, Planet Detection Metrics: Pixel-Level Transit Injection Tests of Pipeline Detection Efficiency for Data Release 25, Tech. rep.
- Christiansen, J. L., Clarke, B. D., Burke, C. J., et al. 2015, *ApJ*, 810, 95, doi: [10.1088/0004-637X/810/2/95](https://doi.org/10.1088/0004-637X/810/2/95)
- Coughlin, J. L. 2017, Planet Detection Metrics: Robovetter Completeness and Effectiveness for Data Release 25, Tech. rep.
- Evans, D. F. 2018, Research Notes of the American Astronomical Society, 2, 20, doi: [10.3847/2515-5172/aac173](https://doi.org/10.3847/2515-5172/aac173)
- Foreman-Mackey, D., Hogg, D. W., & Morton, T. D. 2014, *ApJ*, 795, 64, doi: [10.1088/0004-637X/795/1/64](https://doi.org/10.1088/0004-637X/795/1/64)
- Fulton, B. J., Petigura, E. A., Howard, A. W., et al. 2017, *AJ*, 154, 109, doi: [10.3847/1538-3881/aa80eb](https://doi.org/10.3847/1538-3881/aa80eb)
- Gaia Collaboration, Brown, A. G. A., Vallenari, A., et al. 2018, *A&A*, 616, A1, doi: [10.1051/0004-6361/201833051](https://doi.org/10.1051/0004-6361/201833051)
- Gupta, A., & Schlichting, H. E. 2018, arXiv e-prints, arXiv:1811.03202. <https://arxiv.org/abs/1811.03202>
- Hirsch, L. A., Ciardi, D. R., Howard, A. W., et al. 2017, *AJ*, 153, 117, doi: [10.3847/1538-3881/153/3/117](https://doi.org/10.3847/1538-3881/153/3/117)
- Hsu, D. C., Ford, E. B., Ragozzine, D., & Morehead, R. C. 2018, *AJ*, 155, 205, doi: [10.3847/1538-3881/aab9a8](https://doi.org/10.3847/1538-3881/aab9a8)
- Jenkins, J. M., Twicken, J. D., Batalha, N. M., et al. 2015, *AJ*, 150, 56, doi: [10.1088/0004-6256/150/2/56](https://doi.org/10.1088/0004-6256/150/2/56)
- Kipping, D. M. 2010, *MNRAS*, 407, 301, doi: [10.1111/j.1365-2966.2010.16894.x](https://doi.org/10.1111/j.1365-2966.2010.16894.x)
- Lopez, E. D., & Fortney, J. J. 2014, *ApJ*, 792, 1, doi: [10.1088/0004-637X/792/1/1](https://doi.org/10.1088/0004-637X/792/1/1)
- Mulders, G. D., Pascucci, I., Apai, D., & Ciesla, F. J. 2018, *AJ*, 156, 24, doi: [10.3847/1538-3881/aac5ea](https://doi.org/10.3847/1538-3881/aac5ea)
- Mullally, F., Thompson, S. E., Coughlin, J. L., Burke, C. J., & Rowe, J. F. 2018, *AJ*, 155, 210, doi: [10.3847/1538-3881/aabae3](https://doi.org/10.3847/1538-3881/aabae3)
- Owen, J. E., & Wu, Y. 2017, *The Astrophysical Journal*, 847, 29
- Petigura, E. A., Howard, A. W., & Marcy, G. W. 2013, *Proceedings of the National Academy of Science*, 110, 19273, doi: [10.1073/pnas.1319909110](https://doi.org/10.1073/pnas.1319909110)
- Price, E. M., & Rogers, L. A. 2014, *ApJ*, 794, 92, doi: [10.1088/0004-637X/794/1/92](https://doi.org/10.1088/0004-637X/794/1/92)
- Teske, J. K., Ciardi, D. R., Howell, S. B., Hirsch, L. A., & Johnson, R. A. 2018, *AJ*, 156, 292, doi: [10.3847/1538-3881/aaed2d](https://doi.org/10.3847/1538-3881/aaed2d)
- Thompson, S. E., Coughlin, J. L., Hoffman, K., et al. 2018, *ApJS*, 235, 38, doi: [10.3847/1538-4365/aab4f9](https://doi.org/10.3847/1538-4365/aab4f9)
- Twicken, J. D., Jenkins, J. M., Seader, S. E., et al. 2016, *AJ*, 152, 158, doi: [10.3847/0004-6256/152/6/158](https://doi.org/10.3847/0004-6256/152/6/158)
- Van Eylen, V., Agentoft, C., Lundkvist, M. S., et al. 2017, ArXiv e-prints. <https://arxiv.org/abs/1710.05398>
- Zink, J. K., Christiansen, J. L., & Hansen, B. M. S. 2019, *MNRAS*, 483, 4479, doi: [10.1093/mnras/sty3463](https://doi.org/10.1093/mnras/sty3463)